INFORMATION TO USERS

This manuscript has been reproduced from the microfilm master. UMI films the text directly from the original or copy submitted. Thus, some thesis and dissertation copies are in typewriter face, while others may be from any type of computer printer.

The quality of this reproduction is dependent upon the quality of the copy submitted. Broken or indistinct print, colored or poor quality illustrations and photographs, print bleedthrough, substandard margins, and improper alignment can adversely affect reproduction.

In the unlikely event that the author did not send UMI a complete manuscript and there are missing pages, these will be noted. Also, if unauthorized copyright material had to be removed, a note will indicate the deletion.

Oversize materials (e.g., maps, drawings, charts) are reproduced by sectioning the original, beginning at the upper left-hand corner and continuing from left to right in equal sections with small overlaps.

Photographs included in the original manuscript have been reproduced xerographically in this copy. Higher quality 6" x 9" black and white photographic prints are available for any photographs or illustrations appearing in this copy for an additional charge. Contact UMI directly to order.

ProQuest Information and Learning
300 North Zeeb Road, Ann Arbor, MI 48106-1346 USA
800-521-0600

UMI®

A New View of Mechanotransduction in Bone Cells

by

Lidan You

A dissertation submitted to the Graduate Faculty in Engineering

in partial fulfillment of the requirements for the degree of Doctor of Philosophy,

The City University of New York

2002

UMI Number: 3037457

ProQuest Information and Learning Company
300 North Zeeb Road
P.O. Box 1346
Ann Arbor, MI 48106-1346

This manuscript has been read and accepted for the Graduate Faculty in Engineering in satisfaction of the dissertation requirement for the degree of Doctor of Philosophy.

1/22/2002

Date

Professor Sheldon Weinbaum

Chair of Examining Committee

1-22-2002

Date

Professor Mumtaz K. Kassir

Executive Officer

Professor Stephen Cowin

Professor Susanna[illegible]

Professor Mitchell Schaffler

Supervisory Committee

The City University of New York

Abstract

A NEW VIEW OF MECHANOTRANSDUCTION IN BONE CELLS

by

Lidan You

Mentor: Professor Sheldon Weinbaum

Co-Mentors: Professor Stephen C. Cowin

Professor Mitchell B. Schaffler

Bone adapts readily and rapidly to its mechanical loading environment to give rise to a functionally well designed tissue and organ. The "mechanosensor" for bone adaptation is widely believed to be the osteocyte. However, to date we have only a very preliminary knowledge of how these cells function in this regard. Nevertheless, there is an emerging consensus that strain-induced fluid flow plays a key role in this mechanical signaling. If this is the case, the next key question in understanding osteocyte mechanosensory function then is: How do osteocytes detect this fluid flow? This background is described in Chapter 1.

In Chapter 2, based on fundamental assumptions about the pericellular matrix, its attachment to the cell process and cytoskeletal coupling, we propose a new hypothesis and mathematical model that makes the remarkable prediction that very small strains in live bone created by normal physical activity can be amplified 100-fold at the cellular level. Specifically, the new strain amplification hypothesis proposes that there are transverse filaments in the pericellular matrix surrounding the cell processes which tether the process

to the canalicular wall and also adhesion proteins associated with the cell membrane that link these filaments to the intracellular actin cytoskeleton (IAC). According to this hypothesis, deformation of the IAC due to mechanical loading is caused by bone interstitial fluid flow creating a fluid drag on the transverse tethering filaments which in turn creates a tensile force or hoop tension in the IAC.

In Chapter 3 we describe experiments that confirm and quantify the essential biological elements assumed by this new model using several EM staining techniques. Measurements of the dimensions of osteocytic process and pericellular matrix structure were also performed to provide realistic values for the input parameters that were used in our theoretical model.

Chapter 4 summarizes the important new insights and suggests directions for future research.

Acknowledgements

I would like to express my deepest gratitude to my mentor, Professor Sheldon Weinbaum, who has influenced me greatly. In the past four years, he taught me how to become a real scientist, who always has enthusiasm for the research, instead of just being a person working on research. His enthusiasm for the research and his work style will influence me forever.

Great thanks to my co-mentors, Professors Stephen Cowin and Mitchell Schaffler, for their wonderful scientific advice, careful guidance and encouragement. Professor Cowin has been extremely kind to me. In the past four years, he gave me many wonderful ideas for my research. He is always trying to encourage me. I also learned from him how to pursue science strictly. I really appreciate all he has done for me. Professor Schaffler has opened my eyes to experimental study. His guidance lead me to really appreciate the beauty and toughness of experimental studies. From him, I also learned how to ask questions instead of only caring about the projects assigned to me.

Special thanks to Prof. Susannah Fritton, Dr. Robert J. Majeska, Dr. Melissa Knothe Tate, Dr. Karl Jepsen, Dr. Ozan Akkus, Dr. Lakshmi Rajan, Dr. Anna Polyakova and Dr. Christopher J. Hernandez for their invaluable guidance and advice on my research. I am also grateful to Mr. Damien Laudier and Ms. Valerie Williams who not only have taught me laboratory skills but have also given me much technical assistance.

I would like to thank the staff of the New York Center for Biomedical Engineering, Dr. Mars and Ms. Carol Bamberger, for their great support. I have to mention Liyun

Wang, Xiaping Hu, Peng Guo and all my other fellow graduate students who helped me enormously.

Finally, but not least, I would like to say thanks to my husband, Xiang Long, and my parents for their encouragement and love. Xiang has been always encouraged me through these years. Whenever I have difficulties, he is always there for me and encourages me. Thanks.

This research is supported by NIH grants AR41210 and AR44211, and by grant 668383 from the PSC-CUNY Research Award Program of The City University of New York.

Table of Contents

List of Tables

List of Figures

Chapter 1 Introduction

Bone is a biological system, which keeps adjusting its structure to adapt to its mechanical environment. Mechanical signals are critical for this adaptation process. Of the three types of bone cells, osteoblasts, osteocytes and osteoclasts, osteocytes are believed to be the cells that sense the mechanical load. However, how the mechanical load is sensed remains unknown and is a major area of current research. Some investigators have suggested that osteocytes sense whole tissue strains. However, this view leads to a fundamental paradox, namely, that the strains applied to whole bone (*i.e.*, tissue level strains) are much smaller (0.04% to 0.3%) (Rubin and Lanyon, 1984; Fritton *et al.*, 2000) than the strains (1% to 10%) (You *et al.*, 2000) that are necessary to cause bone signaling in deformed cell cultures. A recent theoretical model developed by the author and coworkers (You *et al.*, 2001), Chapter 2 of this dissertation, provides a potential resolution to this paradox. The model explores the effect of fluid drag forces on pericellular matrix and its coupling to the intracellular cytoskeleton. It is shown that through this coupling the relatively small strain on the tissue level can be amplified 10 to 100 fold at the cellular level and produce strains comparable to *in vitro* studies where intracellular biochemical responses are observed (Murray and Rushton, 1990; You *et al.*, 2000).

To develop the theoretical model in Chapter 2 several assumptions were applied: 1) there is a fluid filled annulus between the canalicular wall and cell process membrane; 2) a pericellular matrix exists in this space and its transverse elements extend from the cell process membrane to the canalicular wall; 3) proteoglycans are the key components of the

pericellular matrix; 4) the pericellular matrix is attached to both the canalicular wall and the process membrane; 5) the osteocyte process has a stiff actin filament bundle that runs axially along its entire length; 6) tensile stress in the transverse filaments can be transmitted by the membrane spanning proteins into this actin filament bundle. However, data to support most of these assumptions are scant. Thus, in Chapter 3 we have developed experimental protocols to observe and measure the pericellular space, the pericellular matrix, the size of the cell process and canaliculus, the hypothesized transverse elements in the pericellular matrix, the proteoglycans in the pericellular matrix, the actin filament bundle in the process, and its cross-linking structure. Experiments on the ultrastructure of osteocytes in adult mice were performed in Dr. Schaffler's laboratory at the Mount Sinai School of Medicine.

1.1 Bone adaptation -- Mechanotransduction in bone

The functional adaptation of bone to mechanical loading is well documented. Mechanical forces due to gravity and locomotion play a vital role in the maintenance of bone mass, its adaptation and formation. Both bed rest and the absence of gravity during space flight lead to bone resorption (Morey and Baylink, 1978), whereas mechanical loading can induce new bone formation (Sessions *et al.*, 1989). However, the mechanism by which bone cells sense and respond to their mechanical environment is not clear. Cowin and Moss (Cowin *et al.*, 1991) provide a summary of the potential excitation mechanisms that were explored prior to about 1990. In these previous studies considerable attention had been focused on stress generated potentials (SGPs) and electric fields as possible excitation mechanisms. The pioneering experiments by Starkebaum *et al.* (Starkebaum *et al.*, 1979)

and Salzstein and Pollack (Salzstein and Pollack, 1987) and the more recent studies by Scott and Korostoff (Scott and Korostoff, 1990) and Otter *et al.* (Otter *et al.*, 1992) have provided detailed information on both the magnitude and phase of the SGPs and their gradients at the osteonal and whole tissue levels. Several models of increasing levels of sophistication have been developed by the our group and others (Salzstein *et al.*, 1987; Weinbaum *et al.*, 1994; Zeng *et al.*, 1994; Cowin *et al.*, 1995) to predict these SGPs and the intracellular electric currents and transmembrane voltages that would be produced by these SGPs (Harrigan and Hamilton, 1993; Zhang *et al.*, 1997; Zhang *et al.*, 1998). While the latter models have been instructive in elucidating the coupling of extracellular and intracellular voltages and electric fields, they do not explain how SGPs lead to intracellular biochemical responses or cellular level activation. Similarly, while bone cells are known to respond to electric fields *in vitro*, the levels of endogenously occurring electric fields produce only very modest intracellular responses (McLeod *et al.*, 1991).

1.2 Potential mechanisms

The difficulties in identifying a suitable cellular signal have led many investigators in the past decade to explore other mechanisms for cellular level mechanotransduction. The two potential physical mechanisms that have attracted the most widespread interest are: (i) bone cells directly sense the deformation of the substrate to which they are attached and (ii) the fluid flow in the lacuno-canalicular porosity of bone (Piekarski and Munro, 1977) can induce a fluid shear stress on the membranes of the osteocyte cell processes that is of sufficient magnitude to induce intracellular signaling (Weinbaum *et al.*, 1994). In either case one is looking for cellular responses that include DNA synthesis, release of

intracellular Ca, second messenger production (e.g. cyclic AMP), release of paracrine factors (e.g., PGE_2), and matrix protein synthesis. For either mechanism the critical question is whether the mechanical forces or deformations encountered *in vivo* are of sufficient magnitude to elicit the intracellular biochemical responses that are observed in cell culture studies. It is the latter question that is the central focus of the present investigation and the motivation for the new hypothesis in You *et al.* (2001), which provides the basis for this study. We, thus, investigate each mechanism more fully below.

1.2.1 Direct substrate deformation

The customary strains in whole bone *in vivo* are typically in the range of 0.01 to 0.3 percent for human and animal locomotion, but seldom exceed 0.2 percent (Fritton *et al.*, 2000; Fritton and Rubin, 2001). If cell membrane stretch occurs as a direct result of surrounding tissue deformation, then strain on osteocyte membranes should be comparable to whole tissue strain. However, *in vitro* studies show that in order to induce any cellular response by direct mechanical deformation of bone cells on flexible membranes, deformations need to be one to two orders of magnitude larger than the bone tissue strains normally experienced by whole bone *in vivo* (You *et al.*, 2000). Similar cell strain magnitudes are needed to activate fibroblasts and chondrocytes (~ 15%) (Almekinders *et al.*, 1993; Guilak *et al.*, 1995), suggesting that in their sensitivity to mechanical strain, osteocytes may not be different from other connective tissue cells. However, in bone the larger strains needed to stimulate osteocytes could not be derived from direct bone matrix deformation since they would cause bone fracture. Thus, in bone there is an inherent contradiction between material and biological stimulation requirements.

Several different approaches have been used to estimate the magnitude of the strain required to produce cellular signaling responses *in vitro*. The paper by You *et al.* (2000) is particularly instructive in that it has helped resolve earlier puzzling and contradictory results by separating out the effects of substrate deformation and fluid shear. The first experiments with flexible membranes in which a positive response was observed (Buckley *et al.*, 1988; Toma *et al.*, 1997) were conducted on cells exposed to strains that were many times that experienced during normal physical activity. Several investigators (Stanford *et al.*, 1995; Zaman *et al.*, 1997) attempted to correct for this by using a different approach in which much smaller deformations were obtained by growing cells on rigid glass slides and exposing the latter to bending deformations in the physiological range. These investigators obtained a positive response, but did not realize that their apparatus introduced a significant fluid shear due to the lateral motion of the slide in the bathing media. Owan *et al.* (Owan *et al.*, 1997) were able to show that the fluid shear was the dominant response in these bending experiments and if this shear was removed there was little response for strains below 8 percent. This was later confirmed in You *et al.* (2000) in controlled experiments with a computer controlled stretch device whose dynamic strain levels could be varied between 0.1 and 10 percent without inducing fluid flow. In the latter experiments there was no change in cytosolic Ca^{++} or osteopontin mRNA levels for substrate strains < 0.5 percent, a value well above the physiological range.

1.2.2 Bone fluid flow and shear stress

The concept that interstitial fluid could flow through the lacuno-canalicular porosity of bone was first introduced in the pioneering paper by Piekarski and Munro (1977). This paper examined fluid flow in bone from a metabolic viewpoint. The authors hypothesized that diffusion alone could not account for the delivery of nutrients and the removal of wastes from the osteocytes in their lacunae and, thus, a convective enhancement was necessary. This metabolic model neglected both the presence of the cell process in the canaliculi and the pericellular matrix surrounding the process, the two critical components in the fluid shear stress hypothesis proposed in Weinbaum *et al.* (1994). In the latter paper it was suggested that fluid flow could also generate a shear stress on the cell process and, therefore, serve as a mechanotransduction mechanism for the excitation of osteocytes by mechanically induced bone fluid flow. In a companion paper, Cowin *et al.* (1995), the case is made that the fibers in the pericellular matrix and the walls of the fluid annulus in the lacuno-canalicular porosity are also the sites of the streaming currents that give rise to the SGPs. The fluid flow model in Weinbaum *et al.* (1994) is combined with electro-kinetic theory in Cowin *et al.* (1995) and the combined theory is used to predict the phase and magnitude of the SGPs produced by mechanical loading. Good agreement with experimental results is obtained when the fiber spacing in the pericellular matrix is between 6 and 8 nm, a spacing that is typical for glycosaminoglycan (GAG) side chains along a protein monomer in proteoglycans. Prior to this hypothesis it was widely believed that the SGPs were associated with small pores in the mineralized hydroxyapatite (Salzstein and Pollack, 1987; Salzstein *et al.*, 1987).

There is currently no experimental technique for directly measuring the *in vivo* magnitude of the fluid flow in bone or the fluid shear stress on the osteocyte processes. One

must currently resort to the theoretical models by Weinbaum, Cowin and coworkers. The striking prediction in Weinbaum *et al.* (1994) is that this shear stress is approximately 0.5 to 3 Pa (5 to 30 dyn/cm^2) or nearly the same as the shear stress that one observes on vascular endothelial cells on the arterial side of the circulation. This is highly counter intuitive since the microvessels are at least two orders of magnitude larger than the fluid annulus that surrounds a cell process. Thus, one might anticipate a much greater flow and shear stress in microvessels. However, the excess pore pressure generated in bone due to mechanical loading is of the order of 1 MPa and thus a 100 fold larger than the vascular pressure. These compensating factors, smaller diameter but larger pressure gradient, lead to a comparable shear stress on the cell process. These theoretical predictions have attracted widespread attention since fluid shear stresses in this range, 0.5-3.0 Pa, have been shown by a number of investigators to elicit intracellular biochemical responses for the mobilization of intracellular Ca^{++} and the expression of mRNA for matrix proteins in both osteoblastic cell lines and MLO-Y4 cells (Reich and Frangos, 1991; Williams *et al.*, 1994; Hung *et al.*, 1995; Jacobs *et al.*, 1998; You *et al.*, 2000). The latter cells maintain an osteocyte-like phenotype and exhibit gap junction connections between cell processes. Recent experiments have also shown that small tracer molecules, such as procion red (300-400 MW), are largely confined to the lacuno-canalicular porosity (Knothe Tate *et al.*, 1998), and that mechanical loading enhances the spread of this tracer (Knothe Tate and Knothe, 2000). In contrast, there is little or no enhancement due to mechanical loading for a 100-kDa dextran (Knothe Tate *et al.*, 2001), suggesting that the GAG in the pericellular matrix serves as a molecular sieve for plasma proteins. The very slow diffusion of procion red into the mineralized matrix is a strong indication that the boundaries of the lacuno-

canalicular porosity are nearly impermeable to water and small solutes except on longer time scales where diffusion has time to act.

1.3 New hypothesis of strain amplification in bone

While this positive response to fluid shear observed in cell culture studies has strongly biased most investigators in favor of the fluid shear hypothesis, there are important differences between fluid flow in live bone and the fluid flow in cell culture, though superficially the *in vitro* model appears to replicate the flow conditions *in vivo*. The model predictions in Weinbaum *et al.* (1994) describe the fluid shear stresses on the membrane of the osteocyte cell processes in their narrow canalicular channels and not on the cell body in its lacuna. The fluid shear stresses in the lacunae are much smaller because of the much larger dimensions of the mineralized structure, which contains the cell body. The lacunae are mixing chambers that enhance the spread of nutrients and tracers during cyclic loading (Wang *et al.*, 2000). At very low Reynolds numbers one does not have convective mixing since there are no fluid flow instabilities that lead to streamline break up and turbulent mixing even though pericellular matrix and canalicular wall roughness are present (Wang *et al.*, 2001). The canaliculi serve as convective conduits for the spread of solutes and the lacunae as reservoirs for irreversible diffusional mixing. Fluid shear studies *in vitro*, thus, cannot duplicate the fluid environment that the osteocyte experiences *in vivo*. In cell culture studies one cannot distinguish between the effects of shear stress on the cell processes and the shear stress on the cell body since both shear stresses are of the same order. This distinction may be critical in the cellular response if the intracellular actin cytoskeleton (IAC) of the cell body and its cell process differ greatly as we describe below.

Cowin and Weinbaum (1998) proposed a novel mechanotransduction mechanism: the strain amplification theory in bone. The concept of the connections existing between the osteocytic cell process and the canalicular wall was introduced for the first time. It was hypothesized that this connections transmit the drag force exerted by fluid flow on the pericellular matrix to the osteocytic cell process membrane and therefore the strain is amplified greatly at the cellular level. However, the intracellular structure of the osteocytic cell process was not considered in this model. Later study revealed that without the intracellular structure, the cell membrane would be exposed to a very large strain that could disrupt the cell.

Based on the model by Cowin and Weinbaum (1998), You *et al.* (2001), for the first time, relate the fluid flow through the pericellular matrix surrounding an osteocyte in its *in vivo* environment and the deformation of the actin cytoskeleton in the cell processes, which we assume are the mechanical sensing arms of the osteocyte. Recent immunofluorescence and field emission scanning electron microscopic studies (Tanaka-Kamioka *et al.*, 1998), have clearly demonstrated that the cell processes have a space-filling actin filament bundle that provides structural rigidity to the process. The theoretical model by You *et al.* (2001) predicts that this tightly packed actin filament bundle has an elastic modulus which is approximately 200 times stiffer than the loose actin filament gel in the cell body. If this prediction is correct, the observed biochemical responses due to fluid shear observed *in vitro* are very likely due to the deformation of the soft actin cytoskeleton in the cell body and not the fluid shear on the cell processes, which are much stiffer. This is strongly suggested by the fact that numerous fluid shear studies on vascular endothelial

cells, which clearly do not have cell processes, respond to fluid shear stresses of the same magnitude as bone cells.

Due to their inaccessibility very little is known about the osteocyte cytoskeleton. All previous studies have been based on conventional demineralized bone tissue (Jande and Belanger, 1971; Weinger and Holtrop, 1974; King and Holtrop, 1975; Palumbo *et al.*, 1990). The recent study by Tanaka-Kamioka *et al.* (1998) is the one exception in which osteocytes have been isolated from embryonic chick calvariae and the three dimensional organization of the cell process observed using field emission scanning electron microscopy (FESEM). These authors point to the striking similarity between the actin filament bundle in the cell process and the filament bundles in columnar epithelia microvilli (proximal tubule and intestine) and the stereocilia of cochlea hair cells, cells whose cytoskeletal organization has been studied much more extensively. The cross-linking molecules, fimbrin, villin and α-actinin, appear to be common to all four cell types (bone, kidney, intestine, hair cells) and the spacing of the cross-linking molecules is similar. This similarity has been the motivation for a detailed comparative analysis of the actin filament bundles in all four cell types and the possible function of these cellular protuberances as mechanotransducers (Weinbaum *et al.*, 2001). This analysis shows that it is very likely that the microvilli in the proximal tubule function as mechanotransducers and are the long sought after afferent sensor in glomerulotubular balance (Guo *et al.*, 2000). Heretofore, only stereocilia have been widely recognized to function in this capacity (Hudspeth, 1992).

These observations have led to a fundamental new view and hypothesis as to how fluid flow in bone may excite osteocytes *in vivo*. This view is supported by experiments

reported herein which show that the cell process is, indeed, a relatively stiff structure and that it is attached to the canalicular wall at regular intervals by transverse pericellular matrix filaments. Theoretical studies reported in You *et al.* (2001), Chapter 2 of this dissertation, predict that the drag forces exerted on these transverse filaments and their side chains are far greater than the integrated fluid shear force on the cell process membrane. Furthermore, the model developed in You *et al.* (2001) predicts that if the transverse elements in the pericellular matrix are linked by membrane spanning proteins and linker molecules to the cytoskeletal actin bundle in the cell process, the latter can undergo deformations that are 20 to 100 fold greater than the whole tissue strains in the mineralized matrix and in the same range as the substrate deformations in experiments with elastic membranes wherein cellular level biochemical responses are observed *in vitro*. The new model thus provides a quantitatively feasible hypothesis as to how the low amplitude strains in living bone can be amplified sufficiently to produce biosignaling responses at the cellular level.

Three assumptions on the ultrastructure of the osteocyte process applied in the model are critical for the validity of this novel theory. First, the pericellular matrix fills the entire pericellular space surrounding the osteocytic process. If the matrix did not fill the entire pericellular space, the flow in the fluid annulus would be highly non-uniform with large variations in fluid shear and drag forces. Second, the transverse elements connect the transverse processes to the canalicular wall. If there were no such connections, deformation of the pericellular matrix could not be transmitted to the intracellular cytoskeleton. Third, an actin filament bundle exists in the osteocytic process. It offers strong resistance to the hoop tension induced by the drag forces on the tethering

filaments in the pericellular matrix. The analysis in You *et al.* (2001) indicates that this more rigid structure is needed to avoid very large cell deformations that would be lethal to the cell.

Some data supporting these assumptions are available in the literature. As to the extracellular component, several EM studies (Wassermann and Yaeger, 1965; Jande and Belanger, 1971; Shapiro *et al.*, 1995) have revealed the existence of a pericellular matrix in the pericellular space surrounding the osteocytic process. Using cuprolinic blue, proteoglycan was stained along the canalicular wall in rat and human bone (Sauren *et al.*, 1992). Proteoglycan has GAG side chains with spacing of 7 nm between them, which makes it the perfect candidate for the molecular sieving component of the pericellular matrix. Transverse elements in the pericellular space were first clearly observed by Shapiro et al. (1995).

With regard to the connection between the pericellular matrix and the process membrane, CD44, a cell surface receptor for hyaluronan, has been localized along osteocyte processes (Hughes *et al.*, 1994; Gohel *et al.*, 1995; Nakamura *et al.*, 1995; Jamal and Aubin, 1996; Noonan *et al.*, 1996).

With regard to the assumption about intracellular components, evidence comes from both *in situ* and *in vitro* studies. *In situ* studies showed densely packed microfilaments fill the entire osteocyte process (Weinger and Holtrop, 1974; Holtrop, 1975; King and Holtrop, 1975). *In vitro* studies revealed the existence of an actin bundle in the osteocytic process (Tanaka-Kamioka *et al.*, 1998) with fimbrin and α-actinin as the linker molecules cross-linking the actin filaments.

Despite extensive research into the ultrastructure of osteocytes mentioned above, major gaps still remain in our knowledge of mature osteocyte ultrastructure. The vast majority of previous *in situ* studies were performed on young animals, whose bone is demineralized so that fixatives can easily diffuse into the tissue in order to obtain cellular structures. It is not known whether similar structures will exist in mature osteocytes. Therefore, in our current study, reported in Chapter 3 in this dissertation, four different fixatives were employed to optimize the preservation of the ultrastructure of osteocytes in mature animals.

Chapter 2 Strain amplification theory in bone

2.1 Introduction

Bone is a dynamic system that can adjust its structure to its mechanical loading. The customary strains in whole bone *in vivo* are typically in the range of 0.04 to 0.3 percent for animal and human locomotion, but seldom exceed 0.1 percent (Rubin and Lanyon, 1984; Fritton *et al.*, 2000). Osteocytes (Fig. 2.1) are believed to be the critical mechanical sensor cells (Cowin *et al.*, 1991; Burger and Klein-Nulend, 1999), although the mechanism by which osteocytes perceive mechanical load is not known. One widely held idea is that cell membrane stretch occurs as a direct result of surrounding tissue deformation. If this is the case, then strain on osteocyte membranes should be comparable to the bone tissue strain. However, *in vitro* studies show that in order to induce any cellular response by direct mechanical deformation of bone cells, deformations need to be one to two orders of magnitude larger than the bone tissue strains normally experienced by the whole bone *in vivo* (You *et al.*, 2000). Similar cell strain magnitudes are needed to activate fibroblasts and chondrocytes (~15%) (Almekinders *et al.*, 1993; Guilak *et al.*, 1995), suggesting that in their sensitivity to mechanical strain, osteocytes may not be different from other connective tissue cells. However, in bone the larger strains needed to stimulate osteocytes cannot be derived directly from matrix deformations, as they would cause bone fracture. Thus, in

bone there is an inherent contradiction between material and biological stimulation requirements. We present here an hypothesis and model to deal with this contradiction.

We consider first the flow of bone fluid due to mechanical loading. Between the osteocyte cell process membrane and canalicular wall is the pericellular space through which the bone fluid flows. A pericellular organic matrix appears to fill the space (Sauren *et al.*, 1992; Aarden *et al.*, 1996). This matrix is supported by transverse fibrils (Shapiro *et al.*, 1995) which appear to anchor and center the cell process in its canaliculus. When a whole bone is deformed, the deformation-induced pressure gradient will cause bone fluid to flow in the pericellular space of the lacunar-canalicular system (Piekarski and Munro, 1977; Weinbaum *et al.*, 1994; Cowin *et al.*, 1995; Knothe Tate and Knothe, 2000) and induce a drag force on the matrix fibers.

As proposed in Weinbaum *et al.* (1994) the fluid flow will also induce shear stress on the cell process membrane. These stresses have been shown to mechanically stimulate bone cells (Reich and Frangos, 1991; Williams *et al.*, 1994). We thus ask which mechanical signal is more important in stimulating osteocytes? If the drag force on the matrix is the larger of the two forces, can it lead to an amplification of the whole bone strain at the cellular level?

Our model leads to two remarkable predictions. First, given an attached pericellular matrix, the fluid drag force on the pericellular matrix (PM) per unit length of cell process will be shown to be more than an order of magnitude larger than the fluid shearing force on the process membrane per unit length. Second, the fluid drag on an attached pericellular matrix can lead to circumferential (hoop) strains in the membrane-cytoskeleton of the cell

process which are up to two orders of magnitude greater than the strains in the mineralized bone matrix.

2.2 Model Development

Our idealized model for an individual canaliculus with its central cell process (Fig. 2.2) is a tube containing a centrally positioned osteocyte process and its surrounding fluid annulus filled with a mesh-like PM.

2.2.1 The PM around the osteocyte process

For the pericellular component, only two structural elements are critical for this mechanical model: 1) a space-filling PM with a fiber spacing Δ that is sufficiently small, and 2) transverse fibrils that tether the cell process to the canalicular wall. From a mechanics point of view, any matrix that has these two characteristics should function equivalently, although the degree of strain amplification will change with the fiber spacing Δ. There is growing evidence to support this basic structure. First, a space filling pericellular matrix surrounding osteocytes is well-established (Wassermann and Yaeger, 1965; Sauren *et al.*, 1992; Shapiro *et al.*, 1995; Aarden *et al.*, 1996). Second, transverse tethering elements were first clearly identified in Fig. 3 in Shapiro *et al.* (1995) and also observed in our own recent EM studies. The pericellular space surrounding the osteocyte process varies from 14 nm to 100 nm (Cooper *et al.* 1966; Weinger and Holtrop 1974; King and Holtrop 1975), depending on animal species and age, age of osteocyte, histological bone type, skeletal location, *etc.* Our own EM studies on adult mice indicate a pericellular space of 30-50 nm. We also observed that the cell process is invariably located

at the center of the canalicular cross-section suggesting that the transverse fibrils are tension elements that anchor and position the cell process within the canaliculus.

Both albumin and proteoglycan exist in the pericellular space (Owen and Triffitt, 1976; Sauren *et al.*, 1992). The effective diameter of albumin is ~ 7nm, similar to the spacing of glycosaminoglycan (GAG) side chains along a proteoglycan monomer (Buckwalter and Rosenberg, 1982). In our previous studies (Weinbaum *et al.*, 1994; Cowin *et al.*, 1995), Weinbaum and Cowin showed that this value of pore size leads to shear stresses of 0.5 to 3.0 Pa for mechanical loads in the physiological range and good agreement with the experimental data for the relaxation time of stress generated potentials (SGP) in bone under four-point bending (Salzstein and Pollack, 1987; Scott and Korostoff, 1990). Thus, in the present work, we assume a PM with a most likely pore size of 7 nm.

Finally, the matrix must be attached to the cell process and the canalicular wall in order for the drag force to be transmitted to the membrane and its underlying intracellular actin cytoskeleton (IAC). If such linker molecules are present, drag forces exerted on the matrix fibers will produce a tensile stress on these linker molecules which, in turn, will produce radial (hoop) strain in the IAC as schematically shown in Fig. 2.2. Possible candidates for these attachment molecules are CD44, laminin, and various integrins (Gohel *et al.*, 1995; Nakamura *et al.*, 1995).

2.2.2 Structure of cell process IAC

Osteocyte processes contain a space filling actin bundle (King and Holtrop, 1975; Tanaka-Kamioka *et al.*, 1998), whose actin filaments are cross-linked at regular intervals along the axis of the process by a linker molecule recently identified as fimbrin (Tanaka-Kamioka *et al.*, 1998) as shown in Fig. 2.2c. The axial actin filaments are ~ 6 nm in

diameter. Fimbrin is also found in intestinal microvilli (Glenney *et al.*, 1981) as well as nonintestinal cell microvilli (Bretscher and Weber, 1980). The typical spacing of fimbrin cross-linked actin filaments in microvilli is ~ 25nm (Chailley *et al.*, 1989). This spacing is consistent with the EM observation in King *et al.* (1975) and Tanaka-Kamioka *et al.* (1998) for an osteocyte process.

2.3 Mathematical Formulation

2.3.1 The drag force on the fibers

The solution for the fluid flow in the fiber filled fluid annulus surrounding the cell process is described in Weinbaum *et al.* (1994). This solution can be used to determine the integrated shear force F_s (Fig. 2b) on the entire cell process membrane,

$$F_s = 2\pi aL \cdot \tau_w = 2\pi aL \cdot \left(\mu \frac{\partial u}{\partial \rho} \right) = 2\pi aL \cdot \frac{\partial p}{\partial R} \frac{b}{\gamma} \left[A_1 I_1 \left(\frac{\gamma}{q} \right) - B_1 K_1 \left(\frac{\gamma}{q} \right) \right] \quad (2.1)$$

Here a is the radius of the osteocytic process, L is the length of the cell process, μ is the fluid viscosity, R is the radial coordinate in the osteon (Fig. 2.3), or the axial coordinate in the canaliculus, ρ is the radial coordinate in the canaliculus, p is the fluid pressure, b is the radius of the canalicular wall, and τ_w is the fluid shear stress on the osteocyte process membrane. The coefficients A_1, B_1, and parameters γ and q are given in Weinbaum *et al.* (1994). I_1 and K_1 are modified Bessel functions of first order. The radial pressure gradient $\frac{\partial p}{\partial R}$ along the axis of the fluid annulus is based on the theory in Zeng *et al.* (1994) for flow in an osteon due to axial loading.

The permeability constant, k_p, used to calculate τ_w here depends on the spacing of the tranverse elements (core proteins) and the GAG side chains along these core proteins. The fiber spacing Δ is the primary determinant of k_p. A simple expression for k_p is derived in Appendix A.

The total drag force (Fig. 2.2b) exerted on the transverse elements between the canalicular wall and the cell process membrane can be obtained by integrating the distributed force, the first term on the left hand side of Eq. (2) in Weinbaum *et al.* (1994), over the fluid annulus

$$F_d = 2\pi\left[\int_a^b \rho\left(\frac{\mu}{k_p}u\right)d\rho\right]\cdot L$$

$$= 2\pi L\frac{\partial p}{\partial R}\left\{\frac{b^2}{\gamma}[A_1 I_1(\gamma) - B_1 K_1(\gamma)] - \frac{b^2}{\gamma q}\left[A_1 I_1\left(\frac{\gamma}{q}\right) - B_1 K_1\left(\frac{\gamma}{q}\right)\right] - \frac{b^2 - a^2}{2}\right\}. \quad (2.2)$$

From Eqs. (2.1) and (2.2) the force ratio F_d / F_s is given by

$$F_r = F_d / F_s = \frac{2q^2[A_1 I_1(\gamma) - B_1 K_1(\gamma)] - \gamma q(q^2 - 1)}{A_1 I_1(\gamma / q) - B_1 K_1(\gamma / q)} - 1. \quad (2.3)$$

Note F_r depends only on the canalicular and fiber geometry and is independent of $\frac{\partial p}{\partial R}$.

2.3.2 Flow-induced strain in the IAC

We next wish to derive a constitutive relation coupling the deformation of the transverse fibrils in the PM and the IAC. In our idealized model sketched in Fig. 2.2d the transverse elements are treated as inextensible but flexible tensile fibers whose load is

transduced across the cell process membrane to its IAC whose effective Young's Modulus is E^*.

a) Force balance on IAC

The constitutive equation for the actin cytoskeleton in the cell process is:

$$\sigma_\rho = E^* \cdot \varepsilon_\rho, \tag{2.4}$$

where σ_ρ is the radial stress in the actin cytoskeleton and ε_ρ is its radial strain.

Although there is extensive literature for determining E^*, these studies, *e.g.*, Satcher and Dewey (1996), Shin and Athanasiou (1999), describe the modulus for the 3-D actin network in the main cell body but not cytoplasmic protrusions, such as microvilli and cell processes. The one exception is the recent model of Guo *et al.* (2000) for the brush border microvilli. Therefore, we have developed, from first principles, a new basic model for the osteocytic cell processes based on the ultrastructure observed in King *et al.* (1975) and Tanaka-Kamioka *et al.* (1998), see Fig. 2.2c. This model for determining E^* is briefly summarized in Appendix B.

The final expression for E^*, Eq. (B5), is

$$E^* = \frac{203EI}{l_2^4} \tag{2.5}$$

where EI is the flexural rigidity of an individual actin filament. Three studies, Oosawa (1977), Kishino and Yanagida (1988), and Dupuis *et al.* (1997) using different experimental techniques indicate that $EI \sim 1.5 \times 10^{-26} Nm^2$. Therefore,

$$E^* = 487.2kPa\,. \tag{2.6}$$

One notes that this value of E^* is two orders of magnitude larger than the measured value for the osteoblastic cell body, 2.5kPa, measured in Shin and Athanasiou (1999). This difference will be discussed later.

b) Interaction between PM and IAC

The radial force balance on the cell process cytoskeleton in Fig. 2.4 is given by

$$P_{equ.} = \sigma_\rho \tag{2.7}$$

where $P_{equ.}$ is the equivalent pressure induced by the tension bearing transverse elements in the pericellular matrix:

$$P_{equ.} = T_\tau / \Delta_1^2 \tag{2.8}$$

Here Δ_1 is the distance between the transverse elements, T_τ is the tensile force exerted by each element, and Δ_1^2 is its associated membrane area. From Eqs. (2.4), (2.7) and (2.8)

$$T_\tau = \Delta_1^2 P_{equ.} = \Delta_1^2 E^* \varepsilon_\rho \tag{2.9}$$

The circumferential hoop strain in the cell process membrane (the change in length per unit original length of the process membrane in the hoop direction) is given by

$$\varepsilon_\theta = \lambda_\theta - 1 = (\rho_1 / \rho_0) - 1 = \varepsilon_\rho \tag{2.10}$$

where ρ_1 and ρ_0 are the radii of the stretched and unstretched membrane, respectively.

c) Force balance on the transverse elements

Due to the high fiber density, the flow in the fluid annulus is a plug flow except for the thin fiber interaction layers that are of order $\Delta/2$ near the boundaries of the fluid annulus. Thus, the drag force exerted on the load bearing fibers in the axial direction can be treated as uniform.

In view of this uniform loading, the equilibrium shape of the transverse element is the well know catenary equation

$$\frac{w_f s}{T_r} = \sinh\left(\frac{w_f d}{T_r}\right) \tag{2.11}$$

where d is the distance between the canalicular wall and cell process membrane. In the present application T_r is the constant radial component of the force exerted by one transverse element on the IAC and w_f is the drag force per unit length on each transverse element. The drag on each transverse element sw_f is obtained by dividing the total drag force on all the transverse elements in the annulus, F_d, by the total number of tensile elements, $2\pi\rho_0 L/\Delta_1^2$, attached to the membrane surface

$$sw_f = F_d/\left(2\pi\rho_0 L/\Delta_1^2\right) \tag{2.12}$$

where s is the total length of the transverse element.

d) Strain on the process membrane

Substituting Eqs. (2.1) and (2.3) into Eq. (2.12), we have

$$sw_f = \frac{F_r \tau_w a \Delta_1^2}{\rho_0} = \frac{F_r \tau_w \rho_1 \Delta_1^2}{\rho_0}. \tag{2.13}$$

Note that τ_w is evaluated from Eq. (28) in Zeng *et al.* (1994) with $a = \rho_1$, and F_d in Eq. (2.12) includes the drag on all the GAG side chains, which can be considered as a distributed force on each transverse element.

From the geometry in Fig. 2.2, the strain ε_θ in Eq.(2.10) is given by

$$\varepsilon_\theta = \frac{s-d}{\rho_0} \tag{2.14}$$

Substituting Eqs.(2.9), (2.10), (2.13) and (2.14) into Eq. (2.11) one obtains

$$\beta \cdot \frac{(1+\varepsilon_\theta)}{\varepsilon_\theta} = \sinh\left[\beta \cdot \frac{(1+\varepsilon_\theta)}{\varepsilon_\theta} \cdot \left(1 - \frac{\rho_0 \varepsilon_\theta}{s}\right)\right], \tag{2.15}$$

or

$$\beta \cdot \frac{1+\varepsilon_\theta}{\varepsilon_\theta} = \sinh\left[\beta \cdot \frac{1+\varepsilon_\theta}{\varepsilon_\theta} \cdot \left(1 - \frac{\varepsilon_\theta}{q-1}\right)\right], \tag{2.16}$$

where

$$\beta = \frac{F_r \tau_w}{E^*} = \frac{F_d}{2\pi\rho_0 L E^*} = \frac{F_d / A}{E^*} = \frac{f_d}{E^*}. \tag{2.17}$$

Here A is the total area of the process membrane, and f_d is the drag force on the fibers per unit area of the cell process membrane. Therefore, β is a new fundamental dimensionless parameter that relates the drag force on the fibers to the elastic properties of the IAC.

In Cowin *et al.* (1995), it was shown that close agreement with experiment could be obtained for both the phase and magnitude of the stress generated potential when q was approximately 2. For $q = 2$, $\rho_0 = s = a = b/2$ and Eq. (2.16) reduces to

$$\beta \cdot \frac{1+\varepsilon_\theta}{\varepsilon_\theta} = \sinh\left[\beta \cdot \frac{(1+\varepsilon_\theta)\cdot(1-\varepsilon_\theta)}{\varepsilon_\theta}\right]. \tag{2.18}$$

Eq. (2.16), or its simplified form, Eq. (2.18), is the basic dimensionless relationship between the hoop strain ε_θ on the cell process membrane and the dimensionless fluid dynamic loading parameter β.

Finally, the strain amplification ratio ε_r is defined as

$$\varepsilon_r = \frac{\varepsilon_\theta}{\varepsilon_b}, \tag{2.19}$$

where ε_b is the strain on the bone surface,

$$\varepsilon_b = \frac{\sigma_b}{E_b}, \tag{2.20}$$

σ_b is the mechanical load on the whole bone and E_b is its Young's Modulus.

2.4 Parameter values

The values of the parameters a_0, q, μ, l and Δ are discussed in detail in Weinbaum *et al.* (1994), Zeng *et al.* (1994) and Cowin *et al.* (1995). It is estimated in the literature that a is typically 50 nm (Cooper *et al.*, 1966; Marotti *et al.*, 1990); note that these references suggest a range of values depending on species, age, histological bone type, and skeletal location). In our study, we have chosen $a = 50$ nm. The radius a_0 of the GAG side chains is 0.6 nm (Curry, 1986) and their most likely spacing Δ along the core protein is 7nm. The length of the GAG is 20 nm and the spacing of the transverse elements is taken to be twice this value, 40 nm, so that the extended GAG forms a space-filling arrangement. The predicted values of q fall within the range $1.5 \le q \le 3.0$ observed in morphometric

studies. In the present work, if not specified, we assume $q = 2.0$, and hence the nominal width of the fluid annulus is $b - a = 50\,\text{nm}$. We also investigate the role of q by looking at the changes of the force ratio, F_r, and hence the dimensionless parameter Δ, when q is changed. The viscosity μ of the fluid in the annulus is 10^{-2} dynes/cm^2, the value of water.

2.5 Results

In Fig. 2.5 we have plotted our solution for the force ratio, $F_r = F_d / F_s$, as a function of the GAG spacing Δ. As shown in Eq. (2.3), F_r is independent of the magnitude and frequency of the mechanical loading and thus an intrinsic property of the matrix and canaliculus geometry. The important result discovered in plotting F_r against Δ was that $F_r >> 1$ over the entire physiological range of Δ (*5~20 nm*). For Δ = 7 nm, the most likely value of Δ, the drag force is *19.6* times larger than the shear force per unit length of cell process. As the fiber spacing increases, the relative importance of the drag force will decrease markedly, and when the fiber spacing $\Delta = 39\,nm$, a non-physiological value, F_d / F_s will be approximately unity.

The effect of frequency on the strain amplification ratio and the absolute strain at different loading magnitudes are shown in Fig. 2.6, where ε_r, given by Eq. (2.19), and ε_θ, given by Eq. (2.14), are both plotted against the loading frequency. The hoop strain is calculated at the position of maximum flow or pressure gradient, which is located at $R = R_i$, the surface of the Haversian canal. Thus, the hoop strain and the strain

amplification ratio shown in Figs. 2.6a, b can be considered as an upper bound. The curves show a monotonic increase in the amplification ratio as a function of frequency for a prescribed loading. One observes that the amplification ratio varies from 19 to 122 and depends significantly on the magnitude of the loading. When the loading magnitude is 1 MPa, corresponding to 50 microstrain at the osteonal lumen, $\varepsilon_r = 122$ at 20 Hz. For this loading the cell process strain is 0.68 percent. For a 20 MPa load (1000 microstrain) at 20 Hz, $\varepsilon_r = 44$ and the cell process strain is 4.9 percent. The corresponding values of ε_r at 1 Hz for a 1 and 20 MPa load are 51 and 19 and the corresponding strains are 0.29 and 2.1 percent, respectively. Strains of the order of 0.3 percent or greater fall in the range where cellular level biochemical responses have been observed *in vitro* in four point bending (Pitsillides *et al.*, 1995).

Fig. 2.7 compares the strains on the process membrane using the measured value for E^* for an osteoblast cell body, 2.5 kPa (Shin and Athanasiou, 1999), and the value for E^*, 487 kPa, predicted by our model for an actin filament bundle. For both cases, the loading on bone is taken as 5 MPa. One can see that using this measured value for the cell body will lead to unrealistically large cell process strains of 25 to 50%. In contrast, our calculation of E^* for an actin filament bundle leads to strains of 1 to 2 percent, which are more reasonable. The large increase in the value of E^* for the actin filament bundle is due to the tight packing of the actin filaments and the close spacing l_2 of the fimbrin cross links. This will be discussed later in Table 2.1.

The relationship between the dimensionless loading parameter, β, and the strain on the cell process membrane, ε_θ defined by Eq. (2.14), is plotted in Fig. 2.8, for ε_θ in the range 0.3 to 8 percent and representative values of q between 1.2 and 6. For the osteocyte

process q lies in the range of 1.5 to 3.0. One of the striking features in Fig. 2.6a is that the strain amplification ratio is a function of loading at a given frequency and decreases as the loading increases, whereas ε_b increases linearly with loading. It is evident from Fig. 2.8 that ε_θ does not increase linearly with β since Eq. (2.16) is non-linear. It is much like pulling a string back on a bow and arrow. The initial deflection is easy and the force required to produce a large displacement increases non-linearly with the applied force.

2.6 Discussion

The effect of fluid drag on PM and the resulting strain on the IAC of the cell process and its plasma membrane are examined for the first time using a combined hierarchical mechanical model. The new model suggests that the small mechanically induced strains on whole bone at physiological loading can be greatly amplified at the cell membrane level, if the fluid drag forces on the PM are transmitted to the IAC in the cell process. This amplification can lead to strains in a range where intracellular biochemical responses have been observed experimentally.

In the past, researchers examining the effect of fluid flow on cells had focused their attention nearly exclusively on the response of cells to fluid shear stress. The drag force exerted on PM fibers has never been considered. However, one observes in Fig. 5 that at a GAG spacing of *7 nm*, the fiber spacing where the matrix could serve as a molecular filter for albumin (Weinbaum, 1998) and the typical spacing of GAG side chains along protein

monomers (Buckwalter and Rosenberg, 1982), the force ratio F_r would be ~ 20 in the fluid annulus. Furthermore, this ratio from Eq.(2.3) is independent of the value of the loading magnitude and loading frequency. This important result suggests that the drag force on the fibers could be the dominant stimulus for the cell's mechanosensory system, rather than, or in addition to, the fluid shear stress on the cell process, as originally proposed in Weinbaum, *et al.* (1994).

Experimental *in vitro* cell culture studies on elastic substrates have typically been performed at strain levels of 1 to 10 percent (Murray and Rushton, 1990). Strain levels in four point bending are significantly lower, 0.38% (Pitsillides *et al.*, 1995). However, the peak levels of the strain on whole bone tissue range from about 0.04 percent to 0.2 percent in humans under varied activities (Lanyon *et al.*, 1975) and 0.04 to 0.3 percent for animal locomotion (Fritton *et al.*, 2000; Fritton and Rubin, 2001). Thus, the strain levels achieved in *in vitro* cell culture studies are much greater than the whole tissue strains experienced physiologically *in vivo*. Klein-Nulend *et al.* (1995) and You *et al.* (2000) have shown that when physiological strains of less than one percent are applied in cell culture, there is no observed cellular response. In contrast, Pitsillides *et al.* (1995) reported rapid increase in NO production at 0.38 percent strain for bone cells in four point bending. However, this load is at the extreme of physiological loading. These observations for bone cells have cast doubt on any previous theory that proposed that cell stretch could be one of the candidates for cell activation in bone.

The new strain amplification hypothesis and model in the present study predict that the strain induced on the whole bone can be amplified by a factor of 20 to 100 or more at the cell membrane level and produce maximum strains from 0.3 to nearly 5 percent on the

cell process membrane for mechanical loading in the physiological range if the drag forces on the PM can be transmitted to the IAC of the cell process. Note also that, for low magnitude- high frequency loads, the amplification effect is significantly greater than for high magnitude-low frequency loads. Eqs. (2.15) or (2.16) and Fig. 8 show that the relation between the drag force on a fiber, $F_d/(2\pi\rho_0 l/\Delta_1^2)$, and the hoop strain, ε_θ, on the process membrane is nonlinear. This could be a factor in explaining why Rubin and McLeod (1996) observed that low magnitude, high frequency mechanical loading appeared to be particularly effective in maintaining bone mass.

The analysis has brought to light a fundamental new dimensionless group, $\beta = f_d / E^*$, relating the drag force on the PM to the elastic modulus of the IAC. In Fig. 8, we have plotted the non-linear relationship between β and ε_θ when ε_θ is in the range 0.3 to 8 percent where one would anticipate an intracellular biochemical response to stretch. The form of Eq. (2.15) and (2.16) is dictated by the deformed shape of the transverse fibrils in the PM which, in this case, is a catenary curve because the loading due to the fluid flow is uniform. A similar expression needs to be developed for an ellipsoidal geometry. This would be useful in describing the flow past the body of the osteocyte in its lacuna or the flow through the matrix surrounding a chondrocyte.

There are several simplifications in the model. We did not consider the change in shape of the fluid annulus or the change in permeability of the PM due to the fluid flow. This change is expected to be small since Δ will not change significantly and the changes in cell process diameter are at most a few percent, see Fig. 6b.

We have also treated the PM as a simple rectangular mesh in calculating k_p. However, one can show that the basic predictions will not change significantly for a

random matrix. The key parameter in determining k_p is Δ. Hu and Weinbaum (2000) have shown that the surface glycocalyx on endothelial cells has sieving properties very close to 7 nm. Our calculation in Table 2.1 shows that if we vary Δ from 5 to 12 nm the strain on the osteocyte process membrane will change by less than a factor of 4 for all frequencies above 1 Hz.

The IAC structure assumed for the cell process is based on numerous histological studies (Weinger and Holtrop, 1974; Holtrop, 1975; King and Holtrop, 1975; Shapiro *et al.*, 1995; Tanaka-Kamioka *et al.*, 1998). The two key parameters are the spacing of the actin filaments, l_1, and the distance between the fimbrin linker molecules, l_2. The variation of l_1 will not greatly change our final results since the strain is induced through bending rather than stretching of the axial actin filaments. l_2 is estimated to be ~50 nm based on the electromicrographs in Tanaka-Kamioka *et al.* (1998) and the fimbrin spacing in the actin bundles of microvilli. Distances larger than this will lead to greater strain amplification. EM studies indicate that l_2 should be larger than l_1 (Shapiro *et al.*, 1995; Horwitz, 1997; Tanaka-Kamioka *et al.*, 1998). l_1 has been taken as 25 nm. The calculations in Table 2.1 for $l_2 = 25nm$ and 100nm indicate that l_2 is a critical parameter in predicting IAC strain. A doubling of l_2 leads to a six fold increase in cell process strain whereas the value of E^* increases as l_2^4, see Eq. (2.5). In contrast, varying the width of the pericellular space, b-a, from 20 to 100 nm produces much smaller strain variations in the IAC, see Table 2.1.

An important insight in formulating the new hypothesis was the realization that the cytoskeleton of the osteocyte process closely resembles the actin filament bundles in the microvilli of the small intestine and proximal tubule (Mooseker and Tilney, 1975; Tanaka-Kamioka *et al.*, 1998). The structural rigidity of this actin filament bundle to bending was

examined for the first time in Guo *et al.* (2000) where it is shown that the brush border microvilli are relatively stiff structures that are well suited to serve as mechanotransducers. One of the crucial observations for the cell process is that it is invariably located at the center of the canalicular cross-section in electron micrographs. Since the cell process is relatively stiff and the canaliculi are seldom straight conduits, it is hard to imagine how such centering can be achieved without there being tensile supporting structures which tether the cell process and its cytoskeleton to the canalicular wall. This indirect evidence led the authors to hypothesize the existence of the transverse elements in the PM, before we were aware that such structures had already been identified in Shapiro *et al.* (1995). Our own recent electron microscopic studies have since confirmed this observation.

Although we have applied the model using pressure gradients calculated for an osteonal geometry, the bone geometry is secondary since the strain amplification mechanism applies at the canalicular level. While the PM is believed to contain proteoglycans (Sauren *et al.*, 1992), this is also non-essential. There are other candidates for the PM, *e.g.*, CD44 molecules with GAG side chains. CD44 has a terminus for hyaluronan, a major component of endothelial glycocalyx. The particular molecules involved are not important in a mechanical model. The results at the cellular level depend only on the canalicular geometry, the fiber spacing and the assumed model for the IAC.

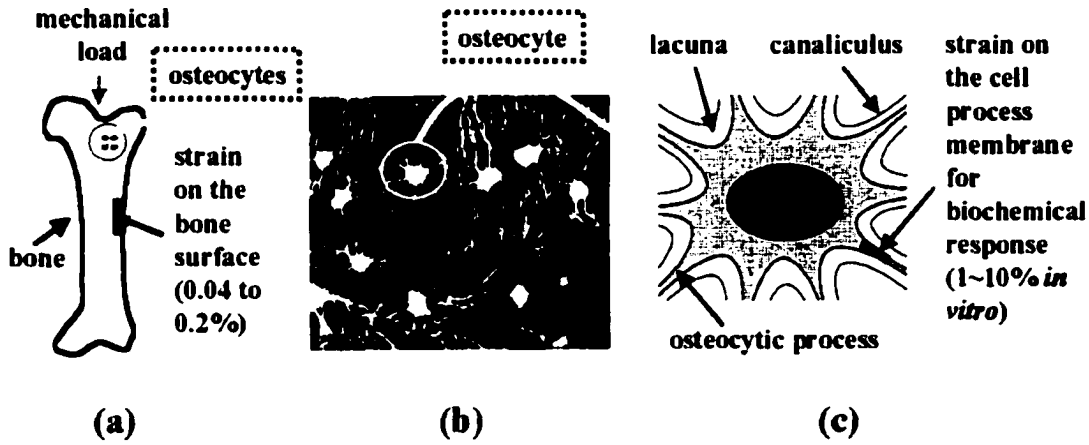

Figure 2.1 This figure illustrates the paradox addressed in this paper. (a) An illustration of the small strains tht the whole bone experiences, strains that are in the range 0.04 to 0.3 percent and seldom exceed 0.1 percent. The last two panels, (b) Photomicrograph of osteocytes encased in bone matrix and (c) Osteocyte in lacuna, illustrate that the whole bone strains in (a) are nearly two orders of magnitude less than those needed (1% to 10%) to elicit biochemical responses *in vitro*, such as an increase in intracellular Ca^{2+} and prostaglandin synthesis. The paradox in the bone mechanosensing system is that the strains that activate the bone cells are two orders of magnitude larger than the strains to which the whole bone organ is subjected.

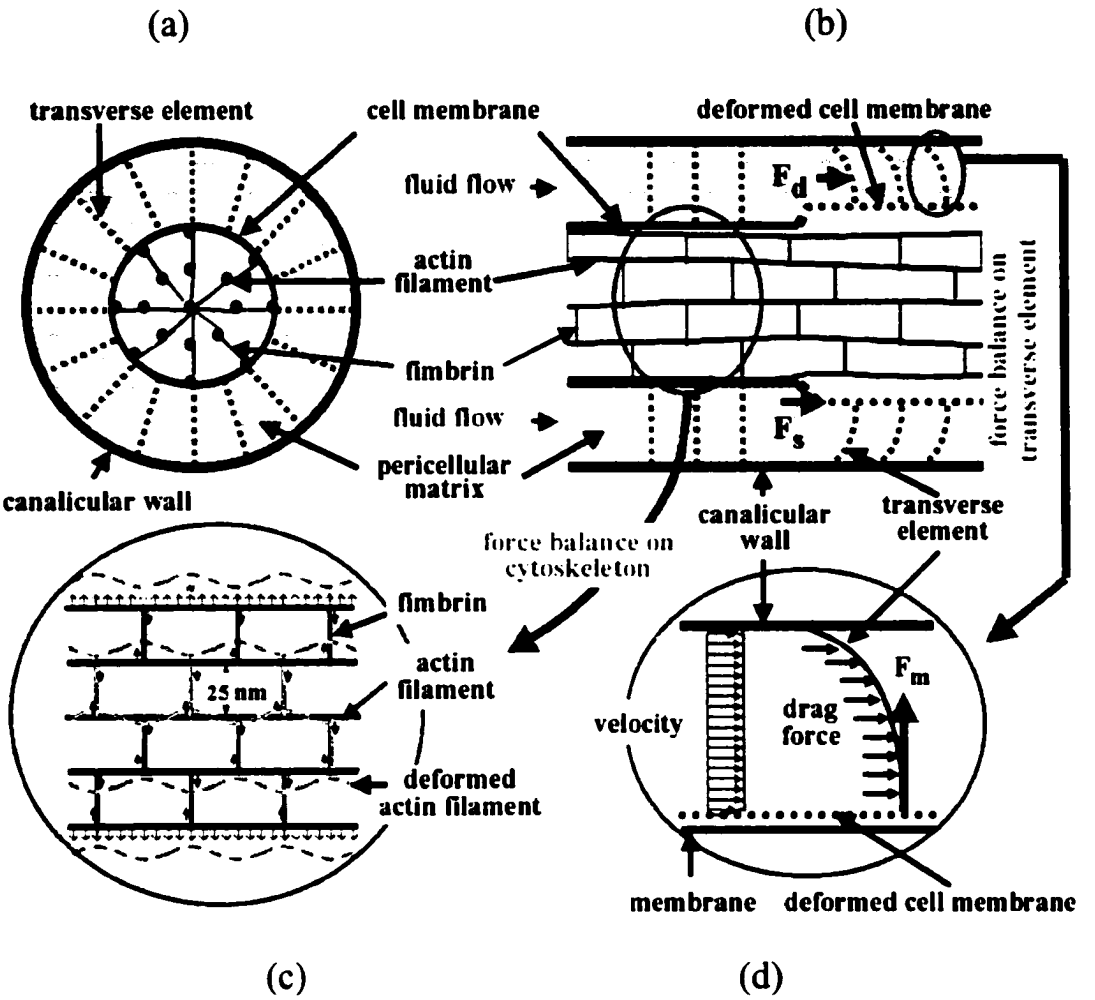

Figure 2.2 Schematic model showing the structure of the PM, the IAC inside the process and the connection between the PM and the IAC. (a) Transverse cross-section of canaliculus showing the fluid annular shape of the region and transverse (radial) pericellular fibers. (b) Longitudinal cross-section before and after the transverse elements are deformed by the flow. (c) Schematic of the cell process cytoskeletal structure in longitudinal axial section used to estimate the Young's modulus in the radial (vertical) direction. Since the length of the cell process is 300 times its radius, it is considered infinite in the longitudinal (horizontal) direction. The axial actin filaments shown are modeled as continuous infinite beams with two types of loadings depending on whether the actin filaments are peripheral or interior. The small vertical arrows indicate the direction of the loading. The (fimbrin) links between these infinitely long beams are considered to be rigid. (d) Force balance on a transverse element.

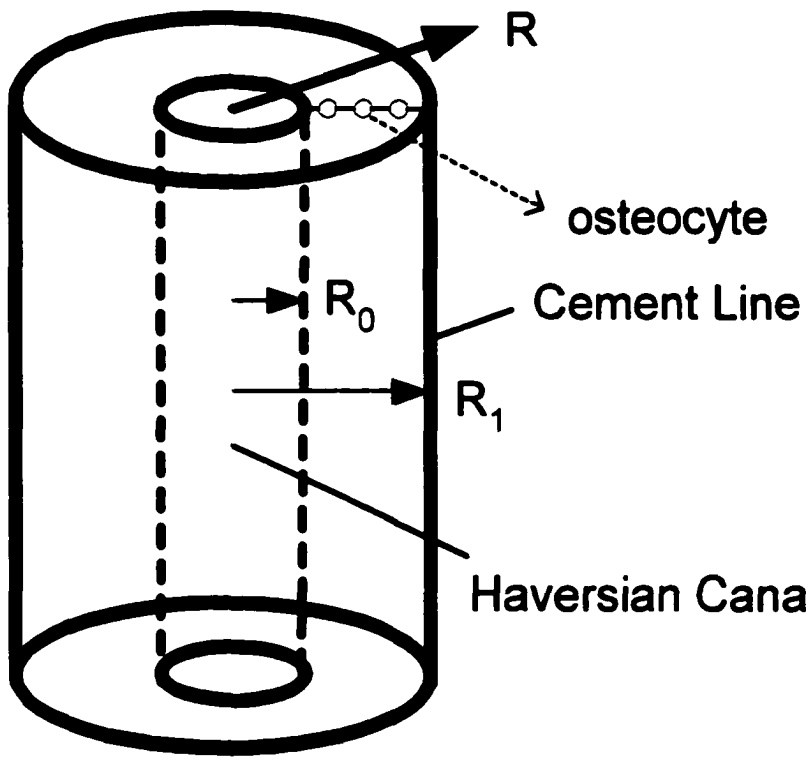

Figure 2.3 Idealized model of an osteonal unit.

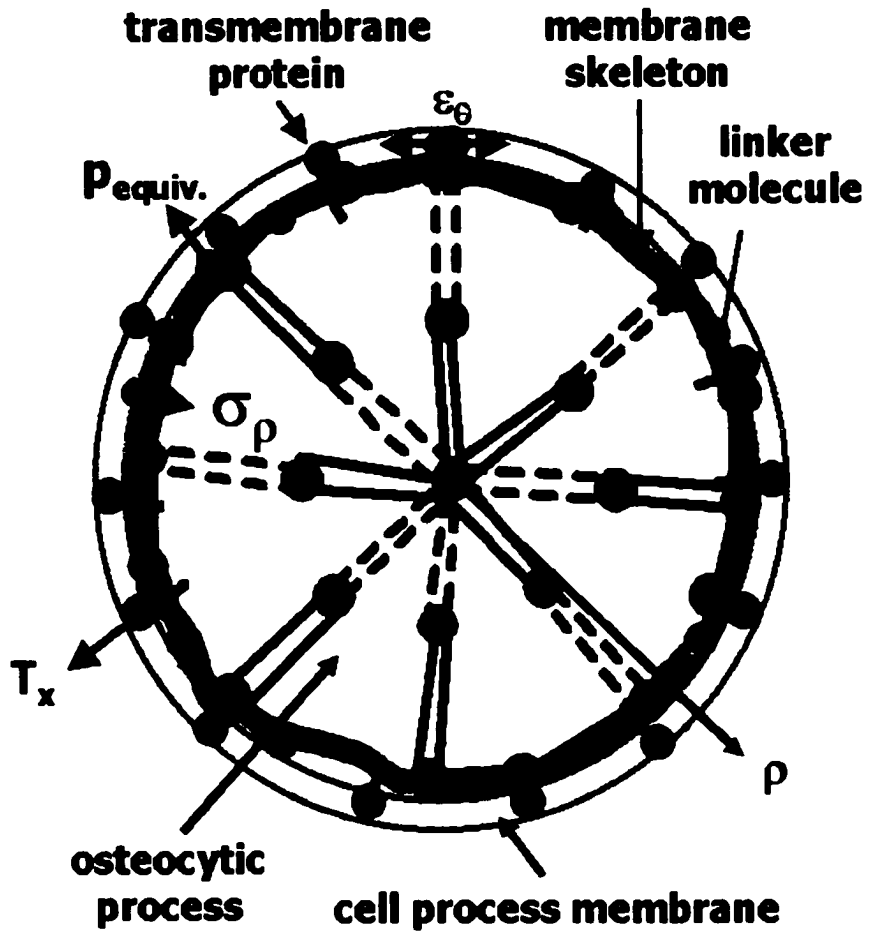

Figure 2.4 Idealized model showing the force balance on the cell process membrane skeleton in transverse section.

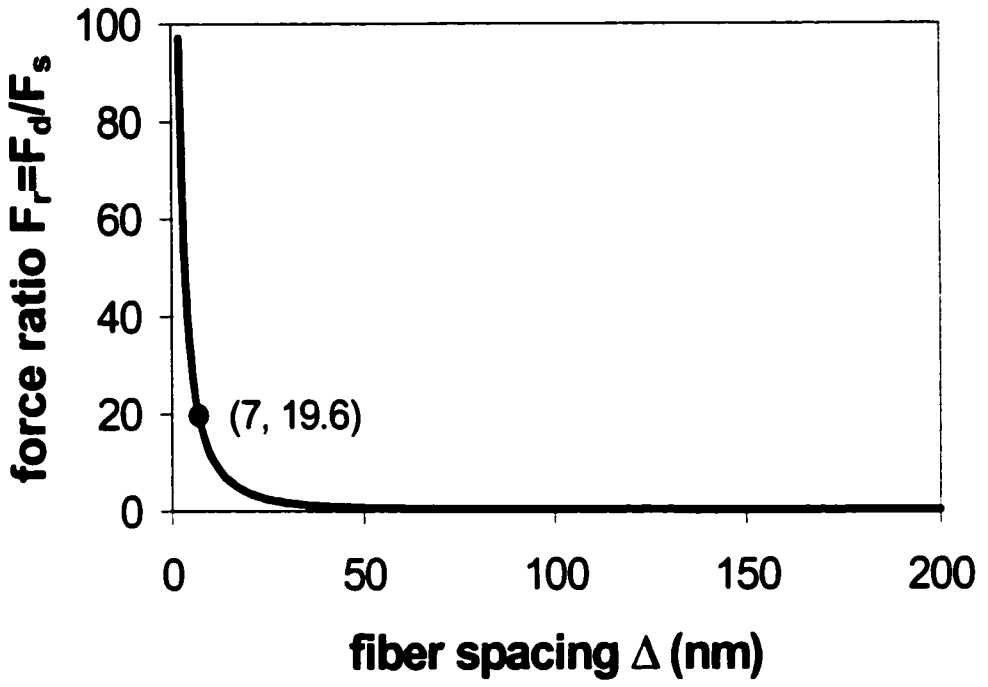

Figure 2.5 The relationship between force ratio F_r and average fiber spacing Δ. Note the force ratio at $\Delta = 7\,nm$ is 19.6. $\Delta = 7\,nm$ is typical of the average spacing of GAG side chains along a core protein and the effective diameter of the albumin molecule which is known to be sieved by an equivalent matrix in capillary endothelium. This varies between 5 and 12 nm. The force ratio F_r is defined as the ratio of the drag force on the fibers to the shear force on the cell process membrane per unit length of cell process.

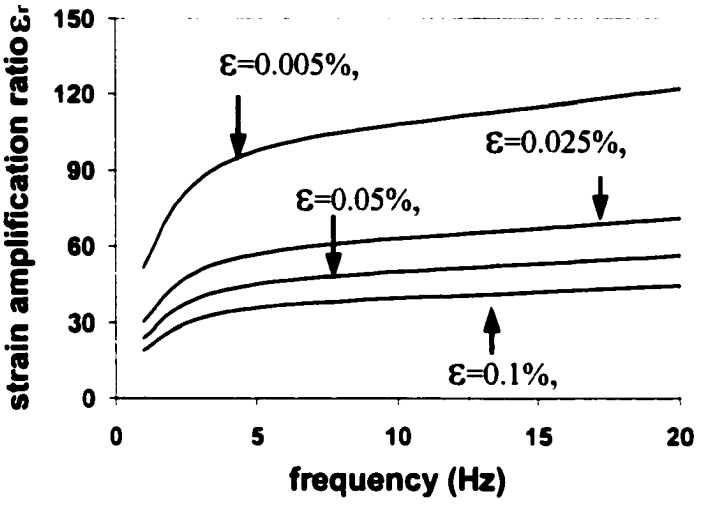

(a)

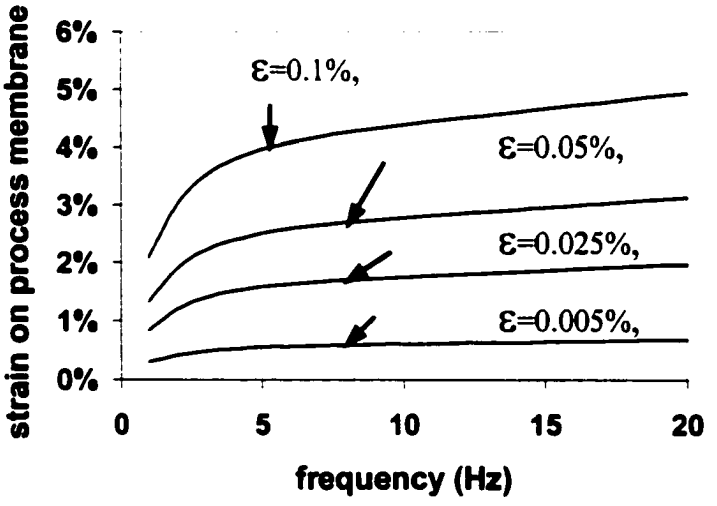

(b)

Figure 2.6 Strain amplification. (a) Plot of the strain amplification ratio ε_r as a function of the load frequency for different load magnitudes. Strain amplification ratio is defined as the ratio of the hoop strain in the cell process membrane to the bone surface strain at the osteonal lumen. ε is the strain on the whole bone. (b) Plot of the cell process membrane strain ε_θ as a function of the load frequency for different load magnitudes. ε is the strain on the whole bone.

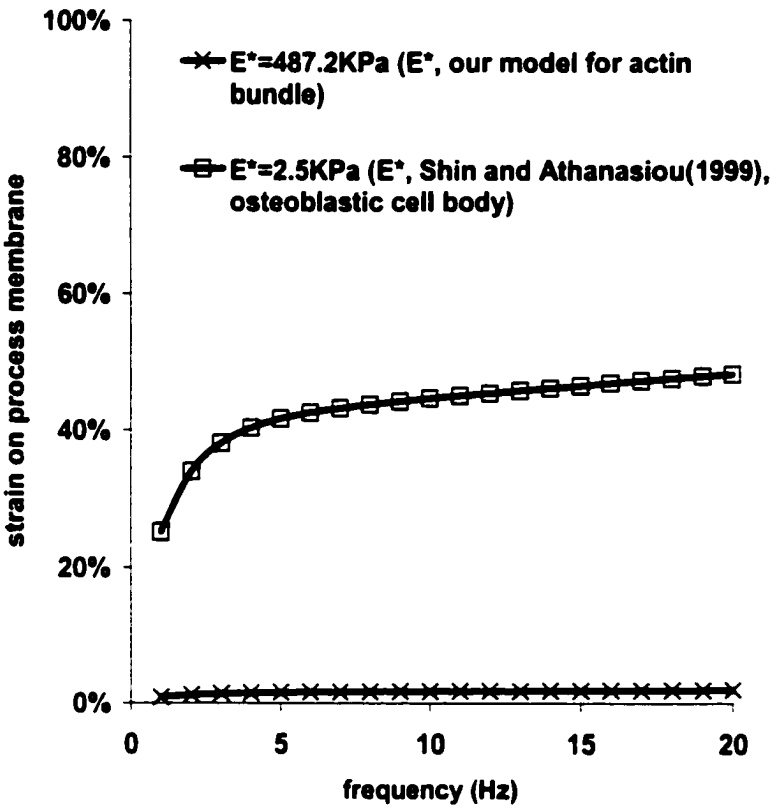

Figure 2.7 The comparison of the strain on the osteocyte process membrane using the measured Young's modulus of the osteoblastic cell body, $E^* = 2.5kPa$ (Shin and Athanasiou, 1999), and our predicted Young's modulus of a closely packed actin filament bundle, $E^* = 487.2kPa$. Both strains are calculated when the loading on bone is 5 MPa.

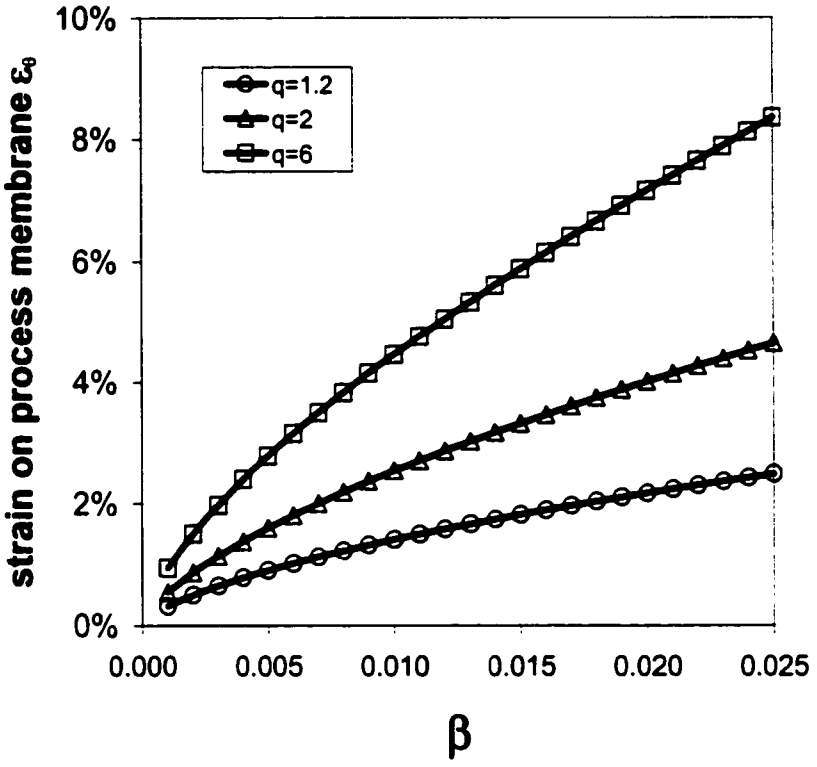

Figure 2.8 The relationship between ε_θ and β when $q = 1.2$, 2 or 6, see Eq. (2.16), where ε_θ is the hoop strain in the cell process membrane and β is a dimensionless loading parameter, defined by $\beta = \frac{f_d}{E^*}$.

		1Hz	2Hz	5Hz	10Hz	20Hz
GAG spacing Δ (nm)	5	1.26%	1.58%	1.82%	2.06%	2.47%
	7	0.83%	1.20%	1.58%	1.75%	1.97%
	12	0.37%	0.59%	0.99%	1.31%	1.51%
Fimbrin spacing l_2 (nm)	25	0.13%	0.19%	0.25%	0.28%	0.31%
	50	0.83%	1.20%	1.58%	1.75%	1.97%
	100	5.23%	7.47%	9.78%	10.8%	12.1%
Width of pericellular space *b-a* (nm)	20	0.60%	0.67%	0.78%	0.94%	1.14%
	50	0.83%	1.20%	1.58%	1.75%	1.97%
	100	0.86%	1.35%	2.26%	2.93%	3.35%

Table 2.1 The predicted values of strains on the osteocyte process membrane obtained for different values of GAG spacing Δ, fimbrin spacing l_2, and width of pericellular space *b-a* when the loading on the whole bone is taken as 5 MPa.

Chapter 3. Experimental studies

3.1 Introduction

In Chapter 2, we developed a novel model (You *et al.*, 2001), which provides a new potential mechanism by which mechanical loading induced fluid flow in the lacuno-canalicular system under routine physical activity can produce deformations of osteocyte processes that are at least one order of magnitude larger than whole bone tissue deformations. This new theory is thus able to explain a fundamental paradox that the larger strains needed to stimulate bone cells cannot be derived from direct bone matrix deformation since they would cause bone fracture. A brief description of this model is given below.

The model assumes the existence of three basic structures: (i) an organic matrix that fills the entire pericellular space surrounding the osteocyte body and the osteocytic processes; (ii) transverse elements that anchor and center the osteocytic process in its canaliculus; and (iii) a cytoskeletal structure within the cell processes to contribute rigidity. When bone is loaded, fluid flow will be induced in the pericellular space of the lacuno-canalicular system due to the deformation induced pressure gradient (Piekarski and Munro, 1977; Weinbaum *et al.*, 1994; Cowin *et al.*, 1995; Knothe Tate *et al.*, 1998; Knothe Tate and Knothe, 2000). The transverse tethering elements in the pericellular space surrounding the osteocytic process can interact with this fluid flow such that a drag force will be exerted on them by the fluid flow.

The resulting deflection of tethering elements, in turn, will be transmitted to the cytoskeleton by membrane spanning proteins and linker molecules producing an outward hoop tension on the osteocytic process membrane. The packed actin filament bundle in the osteocyte process will provide strong resistance to this hoop tension. The balance of these two forces was shown in Chapter 2 to result in a deformation of the cell cytoskeleton that is at least one order of magnitude larger than tissue level strain. Hence, the osteocyte can be subjected to significant local mechanical loading through this coupling mechanism although the tissue level strain is very small.

Several parameter values describing the osteocytic process, pericellular matrix and canalicular structure are required in the model. These include the dimensions of the osteocytic process and canaliculus, the dimensions of the spacing between the transverse tethering elements, the spacing between the axial actin filaments and the spacing of their cross-links.

These assumptions and parameter values are critical for the validity of the model and its quantitative predictions. Existing morphological data to support these assumptions and provide the parameter values are scant. While there is a large body of experimental studies investigating various aspects of the ultrastructure of osteocytes and their pericellular space (Weinger and Holtrop, 1974; Holtrop, 1975; King and Holtrop, 1975; Sauren *et al.*, 1992; Shapiro *et al.*, 1995), most of these studies were performed on recent formed osteocytes in tissue from very young animals. Moreover, even the fundamental question of the existence of a pericellular space, a space which is essential for the function of all fluid flow based theories of osteocytes mechanotransduction, remains unresolved. It is not known whether osteocytes in mature bone have the same cytoskeletal and pericellular matrix structure as in immature bone, or for that matter, even whether the canalicular boundary is fully mineralized. As such

information is critical for the validity of the new theory in You *et al.* (2001), new experimental studies were conducted to examine these assumptions using improved ultrastructural techniques. The current studies were designed to investigate the ultrastructure of mature bone samples to: 1) verify the existence of the pericellular space in the fluid annulus surrounding the cell process and quantify its dimensions; 2) verify the existence of the transverse elements in the pericellular matrix; 3) visualize the axial microfilaments inside the osteocyte cell processes and obtain initial estimates of their number density and spacing; 4) quantify the cell process and canalicular diameters; 5) quantify the spacing between transverse elements in the pericellular matrix and the spacing between the actin filaments in the process. The measurements in 4) and 5) will provide critical input data for osteocyte ultrastructure that is important for obtaining realistic quantitative predictions using theoretical model described in Chapter 2. These data are also important input for all theoretical models on the interstitial fluid flow in the lacuno-canalicular porosity in bone.

3.2 Materials And Methods

Studies were performed on humeri of 3 fifteen-week old BalB/cByJ female mice (N=3; 21~24g). The cortical bone diaphysis was cut into 1 mm thick cross-sections. After the removal of the bone marrow, the samples were immediately immersion fixed. It is widely supposed that the pericellular material surrounding osteocytes processes is proteoglycan. These molecules are notoriously difficult to fix for microscopy study. Hunziker *et al.* (1982) showed that by adding Ruthenium III Hexammine Trichloride (RHT) to the primary aldehyde fixatives, the preservation of proteoglycans in cartilage could be improved greatly. The

principal advantage of using ruthenium-containing fixatives is that they avoid the creation of a pericellular lacunar space by preserving the interconnected nature of matrix proteoglycans and the integrity of the latter with the chondrocyte plasma membrane and matrix vesicle membranes. With RHT, the fixatives will be able to penetrate tissue blocks to a greater depth and in a more homogenous manner than ruthenium red only. Thus, in the current ultrastructural studies RHT is combined standard fixative procedures in order to access whether this combination will provide new information on the proteoglycan structure surrounding the osteocytic process.

The samples were fixed for 24 hours in one of the following four groups of fixatives: 1) Primary fixation media with glutaraldehyde only – group G (2% glutaraldehyde in 0.05M cacodylate buffer at 7.4 pH); 2) Primary fixation media with glutaraldehyde and RHT –group GR (2% glutaraldehyde in 0.05M cacodylate buffer at 7.4 pH containing 0.7% RHT); 3) Primary fixation media with glutaraldehyde and paraformaldehyde –group GP (2% glutaraldehyde and 4% paraformaldehyde in 0.05M cacodylate buffer at 7.4 pH); 4) Primary fixation media with glutaraldehyde, paraformaldehyde and RHT–group GPR (2% glutaraldehyde and 4% paraformaldehyde in 0.05M cacodylate buffer with 0.7% RHT at 7.4 pH).

The specimens were then decalcified using 10% EDTA in 0.1M Tris-HCL buffer for two weeks. Prior to postfixation, tissue blocks were washed for 3 x 5 min in the Tris buffer. Postfixation was then carried out in 1% osmium tetroxide in Tris buffer. During all processing steps, the RHT and identical pH were maintained. The specimens were then washed in PBS, dehydrated in graded ethanols, and infiltrated for one week in a mixture of epon and pothylene oxide (Weinger and Holtrop, 1974). Specimens were embedded in epon

with the longitudinal axis of the bone parallel to the sectioning surface so that optimal registration of cross or longitudinal sections of osteocyte processes could be obtained. Ultra thin sections were cut with a diamond knife and stained with a saturated solution of uranyl acetate in 50% ethanol followed by 0.2% lead citrate. The sections were placed on Parlodion-coated 200-mesh copper grids and viewed with a Philips EM 300 electron microscope.

All ultrastructural measurements were made directly from micrographs and performed by a single investigator. Data are shown as mean ± standard deviation.

3.3 Results

Four groups of fixatives were used in the current studies. The glutaraldehyde appeared to be unsuitable. It was able to preserve only the transverse elements in the pericellular space surrounding the osteocyte process while all the other components of the cellular structure were lost. When the glutaraldehyde was combined with a high penetrating fixative, paraformaldehyde, cellular structures such as the cell membrane and the cytoskeleton were preserved. When the glutaraldehyde was combined with RHT, the pericellular matrix was well preserved while the intracellular structure was lost. The best preservation was obtained when the three fixatives were employed together, which was GPR.

1. Pericellular space and the dimensions of the osteocytic processes, the canaliculi and the pericellular space. Transverse sections of osteocyte processes were always found to be surrounded by a pericellular space and symmetrically centered within the canaliculi (Fig 3.1).

The present of a uniformed distributed pericellular matrix surrounding the osteocyte process and filling the entire space suggests that the pericellular space is indeed a real space and not a shrinkage artifact. An enlarged cross section of an osteocyte process is shown in Fig. 3.2, group GPR. One can see that the pericellular matrix entirely surrounds the process and the canalicular wall is darkly stained by the RHT. If the pericellular space results from shrinkage, no matrix would be observed in this space. Measurements of the dimensions of the processes, the canaliculi and the pericellular space were made on transverse sections of canaliculi. We measured the diameters of the osteocytic processes and the canaliculi directly from the cross sections canaliculi. These micrographs are taken on bone samples from all four fixative groups. Results are shown in Fig. 3.3. Diameters vary from 50 to 410 nm for the osteocytic process diameter and 80 to 710 nm for the canaliculus diameter. The measured average diameter of the canaliculi was 259 ± 129 nm. The average diameter of the cell process was 104 ± 69 nm. Using these data, the average width of the pericellular annulus is 78 ± 38 nm.

2. Transverse tethering elements and the spacing between them. Transverse elements were found span the entire pericellular space from the process membrane to the canalicular wall. They are visible at both cross and longitudinal section. These elements were dense and were arranged in a periodic fashion (Fig 3.4, 3.5). Measurements of the spacing between these transverse elements were made on both longitudinal and transverse sections of canaliculi. The transverse elements can be clearly seen in the pericellular space surrounding the osteocytic process. The number of the transverse elements were counted. The spacing between the transverse elements was calculated by dividing the length or perimeter of the section by the number of transverse elements the portion of the longitudinal/transverse section contained and

the magnification. Results are shown in Fig. 3.6. The spacing varies from 12 to 76 nm in longitudinal direction and 20 to 115 nm in cross sectional direction. The mean value for this spacing was 38 ± 21 nm for longitudinal section and 41 ± 24 nm for transverse section. Statistics analysis (ANOVA) showed that the spacing from longitudinal sections and transverse sections is not significant different ($P>0.05$). Precise measurement of transverse element spacing can not be obtained from the current studies, as these measurements include some volume projection effects due to the section thickness. However, section thickness correction can be estimated, assuming the distance between transverse elements are the same at both longitudinal section and transverse section, the average spacing is increased by about only 20%.

3. Microfilaments in cell processes and the spacing between the filaments.

Microfilaments were observed in the osteocyte process in both longitudinal sections where they appear as axial filaments (Fig. 3.4) and transverse sections, where they appear as small darker spots inside the process (Fig. 3.2 and Fig. 3.7). Diameters of microfilaments within the osteocyte process were measured directly from electron micrographs. Results are shown in Fig. 3.8. Diameters vary from 2 to 13 nm. The mean value of the measurements for the microfilament diameters was 7 ± 3 nm. The spacing between the axial microfilaments was evaluated from transverse sections of osteocytic processes. The diameters of the osteocytic processes were measured, and the cross sectional areas were calculated based on these diameters assuming a circular profile. The number of the actin filaments in each cross section were counted. Dividing the cross sectional area of the osteocytic process by the number of the microfilaments within the cross section, one obtains the average area each microfilament being surrounded. The diameter of this effective circular area can be taken as the spacing

between the microfilaments. The actual spacing was calculated by dividing this effective diameter by the corresponding magnification. Results are shown in Fig. 3.9. The values vary greatly and range from 20 to 80 nm. The mean value of the measurements for the spacing between the microfilaments was 32 ± 14 nm.

3.4 Discussion

These experimental studies confirm the existence of the fundamental microstructural features needed for strain amplification to occur in loaded bone (Chapter 2). In addition, these measurements for the key structural dimensions are in excellent agreement with the assumed parameter values in our theoretical model (You *et al.*, 2001). These data are also critical for all theoretical models involving fluid flow in the lacuno-canalicular system of bone.

The fundamental ultrastructural features assumed in the theoretical model described in Chapter 2 are: 1) The existence of the pericellular space; 2) The presence of a spacing filling pericellular matrix; 3) The existence of the transverse tethering elements in the pericellular space; 4) the presence of a space filling actin filament bundle in the cell process. The key parameters required in the theoretical model are: 1) The dimensions of the canaliculi, the osteocytic processes and the pericellular space; 2) The spacing between the transverse tethering elements; 3) The spacing between the axially oriented microfilaments. These assumptions and parameter values are discussed below.

While the majority of the researchers believe that there is a pericellular space surrounding the osteocytic process in the canaliculus, there is no complete agreement on this issue. Many theoretical models involving fluid flow in the lacuno-canalicular system have been constructed based on the assumption that the cell process is surrounded by a pericellular

space (Salzstein *et al.*, 1987; Weinbaum *et al.*, 1994; Zeng *et al.*, 1994; Cowin *et al.*, 1995; Wang *et al.*, 1999; Wang *et al.*, 2000). Indirect evidence is obtained from studies (Knothe Tate *et al.*, 1998; Knothe Tate and Knothe, 2000; Knothe Tate *et al.*, 2001; Wang *et al.*, 2002) in which the penetration of different size molecular tracers into the lacuno-canalicular system is observed after the tracer is injected into the animal's vascular system.

However, some investigators still express concern as to whether the pericellular spaces observed in bone are artifacts, a result of shrinkage due to fixation (Wassermann and Yaeger, 1965; Weinger and Holtrop, 1974; Shapiro *et al.*, 1995). Since all the previous observations on the pericellular space were conducted on young animals, the question also remained as to whether this space exists in mature animals. Prior to this study, these questions had not been addressed. In the current studies, the existence of the pericellular space is clearly demonstrated in mature animal bone. The pericellular space observed in our study appears to exist the in living state and is not an shrinkage artifact. If the space was an artifact due to shrinkage, then the space should appear empty on the micrograph. In our studies the pericellular space is always filled with matrix, which is particularly well preserved by a combination of high penetrating fixative (GP) and cationic fixative (RHT). The inclusion of RHT works so effective to preserve the matrix content of the pericellular space. This observation is in great favor of the idea of the proteoglycan forms the majority constituent of the pericellular matrix (Hunziker *et al.*, 1982). The existence of pericellular space is one of the key assumptions in all theoretical models involving fluid flow in the lacuno-canalicular system of bone.

These studies demonstrate the existence of the transverse tethering elements connecting the osteocytic process to the canalicular wall. In the cross sections of canaliculi osteocytic processes always appear in the center of the canaliculi. If there were no connections

between the osteocytic processes and the canalicular wall, the processes would be located randomly inside the canaliculi instead of always being centered within the canaliculi, strongly suggesting that the osteocytic processes are fixed in the central position relative to canalicular wall. In the current studies the transverse tethering elements can be clearly observed in both longitudinal and transverse sections of the canaliculi. Prior to the present study the existence of transverse elements was only mentioned anecdotedly in Shapiro *et al.* (1995). You *et al.* (2001) infers the existence of transverse tethering elements from a functional viewpoint based on the ubiquitous centering of the cell processes without direct supporting histological evidence on the existence of the tethering filaments. Our experiments thus confirm for the first time the existence of transverse tethering elements in the pericellular space in mature animal bone. The important observation for our theoretical model is that the transverse fibers span the entire pericellular space and provide direct linkage of the osteocyte process with the canalicular wall. With this structure, the drag force exerted on the pericellular matrix can be transmitted to the actin filament bundle within the cell process to induce cell deformations that are of sufficient magnitude to be sensed by bone cells and elicit an intracellular signaling response.

While our studies strongly suggest that the osteocytes are tethered to the canalicular wall through the transverse elements, the identity of the transverse elements and the connections between these transverse elements and the intracellular structure is unclear. Possible candidates for the attachment molecules for this tethering are CD44, laminin and various integrins. CD44, which is a cell surface receptor of HA, has been found on the surface of osteocyte (Hughes *et al.*, 1994; Nakamura *et al.*, 1995; Jamal and Aubin, 1996; Nakamura and Ozawa, 1996; Noonan *et al.*, 1996). Specifically, Noonan *et al.* (1996) labeled both HA

and CD44 along the canaliculi. Moreover, the estimated extracellular part of CD44 is approximately 40 nm long, while the pericellular space surrounding the osteocyte process is measured to be 80 nm in average in our studies. In the light of these observations, CD44 might be the best candidate for the tethering elements that connect the process to the canalicular wall.

The present data are the first measurements of the spacing between the transverse tethering elements. The present study is the first wherein the transverse elements were seen with sufficient clarity for this spacing to be measured quantitatively. The average measured spacing is 38 nm at longitudinal section and 41 nm at cross section. This spacing of tethering elements is in the range predicted by You *et al.* (2001) to induce strain amplification, and is consistent with the prediction that the tethering filaments might be CD44 since the typical length of GAG side chains is 20 nm. In our theoretical model, we assumed a spacing of 40 nm, which is twice the length of the GAG side chains. A typical spacing of protein monomer binding sites along HA is 30-40 nm (Lodish, 1999).

There have been a number of studies showing the presence of microfilament bundles in the osteocytic process in young animals (Weinger and Holtrop, 1974; Holtrop, 1975; King and Holtrop, 1975). In 1998, the immuno-histochemical *in vitro* study by Tanaka-Kamioka *et al.* (1998) showed the existence of actin filament bundle in the osteocytic process with fimbrin and α -actinin as linker molecules between the actin filaments. However, the question remained as to why this structure was needed and whether it exists in mature osteocytes. In the development of our theoretical model, we concluded that a significant stiffer cytoskeletal structure must exist inside the osteocyte process than in the cell body to balance the strong drag force transmitted from the pericellular matrix to the cytoskeleton so that reasonable

deformations of the process can be obtained. This consideration was the motivation for our experimental investigation of the presence of the actin filament bundle in mature osteocyte process. Our observations of microfilaments inside the process confirm the existence of a filament bundle structure in mature osteocytes and provide support for this aspect of our model. The microfilament diameters that we measured is 7 ± 3 nm, which is typical of the diameter of F-actin. However, an immuno-histochemical study is needed to make a definitive identification.

With regard to the spacing between the axial microfilaments in the cell process, there is no mention at all of this parameter in the literature. The only related data that we could find is the data from similar structures in the microvilli in the kidney and intestine and in the hair cells in the inner ear (Weinbaum *et al.*, 2001). All three of these structures have axial actin filament bundles as their central cytoskeleton with either fimbrin, villin or α-actinin as the common linker molecules between the actin filaments. The spacing between the actin filaments varies from 12 nm in stereocilia to 25 nm in kidney microvilli. The latter is very close to the approximately 32 ± 14 nm space that we measured in the osteocytic process. This measured spacing, is also in good agreement with the value, 25 nm, we assumed for the distance between the microfilaments in our theoretical model, You *et al.* (2001). At present we have not yet been able to obtain the resolution needed to determine the three dimensional arrangement of the actin filaments and their linker molecules, fimbrin and α-actinin.

The key parameters in all theoretical models involving fluid flow in the lacuno-canalicular porosity are the dimensions of the canaliculi, the osteocytic processes and the pericellular space surrounding the osteocytic process. These parameters influence the results of calculations (e.g., the shear stress on the osteocyte process membrane, the streaming

potential) greatly. Although there are many ultrastructural studies showing micrographs of osteocyte processes in canaliculi, there is no systematic quantitative study of these parameters. Moreover, there is lack of agreement between researchers on the reported values of these parameters. For the sake of comparison, we extracted canaliculi and processes from the literature, either using published measurements or by performing our own measurements on the published photographs (Table 3.1, 3.2). The process and canalicular diameter varies depending on animal species and age. Values of these parameters were also predicted in some theoretical models from a functional viewpoint. Kufahl and Saha (Kufahl and Saha, 1990) pointed out in their theoretical model that the canalicular diameter should fall in the range 100 nm to 800 nm. Their calculations suggest that the canalicular diameter should be ~200 nm to satisfy metabolic requirements. However, they neglect the presence of the cell process.

From the above analysis, one concludes that the size of the canaliculi and the osteocytic process may depend greatly on animal age and animal species. However, none of these studies was quantitative. The credibility of these data are thus in doubt. Therefore, we have performed a detailed quantitative investigation of these parameters in one adult animal species, mice. As the first step of the investigation, this study has not yet examined the effects of animal age and animal species.

To our knowledge, this is the first time that RHT has been utilized in the primary fixation of bone tissue. We found that in addition to improving fixation of the matrix in the annular space, RHT provides a very pronounced staining of the canalicular wall, which appears as a condensed dark region. We believe this dense region is due to the aggregation of the proteoglycans along the canalicular wall, consistent with the crystalline staining of GAG's at this surface using cuprolinic blue that was reported by Sauren *et al.* (1992). The width of

the fluid annulus surrounding the cell process would be nearly the same in traditional and RHT staining methods if the thickness of this condensed black line were taken into account. The average measured canalicular diameter was 259 nm. The average measured process diameter was 104 nm. From these two values, one can calculate the width of the pericellular space, which is 78 nm. Comparing these results with the corresponding parameter values assumed in You *et al.* (2001), 200 nm for the canalicular diameter, 100 nm for the process diameter and 50 nm for the pericellular space, and considering the sensitivity analysis given in that paper, one concludes that the parameter values used in the theoretical model are reasonable, though the assumed width of the pericellular space is on the low side.

This is the first time that a quantitative study has been conducted on the dimensions of the canaliculi, the osteocytic process and the pericellular space surrounding the osteocytic process for any animal species. The measured values of these parameters are important input parameters in any theoretical model for fluid flow in lacuno-canalicular system. However, even for one species confined to only adult animals there is still great variability in the data. We do not know whether this is the intrinsic property of the osteocyte processes and the canaliculi, or it is the results of a limited sampling. Further investigations are needed to clarify this question.

In conclusion, the present experiment provides the most complete existing data for the pericellular space, the pericellular matrix, the transverse elements in this matrix, and the actin filament bundle observed around and in mature osteocytic processes. All these factors are critical for the novel hypothesis proposed by You *et al.* (2001): the existence of the pericellular space is critical for the fluid flow in the lacuno-canalicular system; the existence of the pericellular matrix will allow the drag force being induced; the transverse tethering

elements will transduce the drag force into the actin filament bundle within the process; and the actin filament bundle will offer the resistance to the drag force so that the osteocyte process will not be over stretched while at the same time the strain on the process is large enough, which allows the mechanical signal to be sensed by the osteocyte process. Therefore, the observations in current studies strongly support the theoretical model in which a fundamental new view was advanced for mechanotransduction and strain amplification in bone cells (You *et al.*, 2001). In addition, several key structural parameters were measured, which provide important input data for future models describing mechanotransduction in bone.

Figure 3.1 Electron photomicrograph showing several longitudinal and transverse cross sections of osteocyte processes. The central positioning of the processes in the canaliculi can been clearly seen. **A**. Longitudinal section of a canaliculus with cell process at its center. The black line is the canalicular wall. **B**. Transverse cross section of a canaliculus with cell process at its center. The black line along the circle is the canalicular wall. Bar = 1 μm.

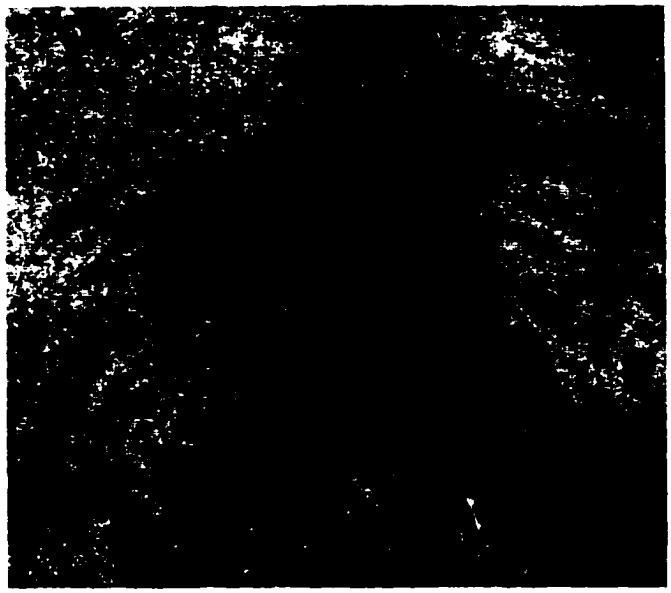

Figure 3.2 Electron photomicrograph showing the cross section of an osteocyte process, with pericellular matrix surrounding the osteocyte process. Paraformaldehyde-glutaraldehyde-RHT fixed. Bar = 100 nm.

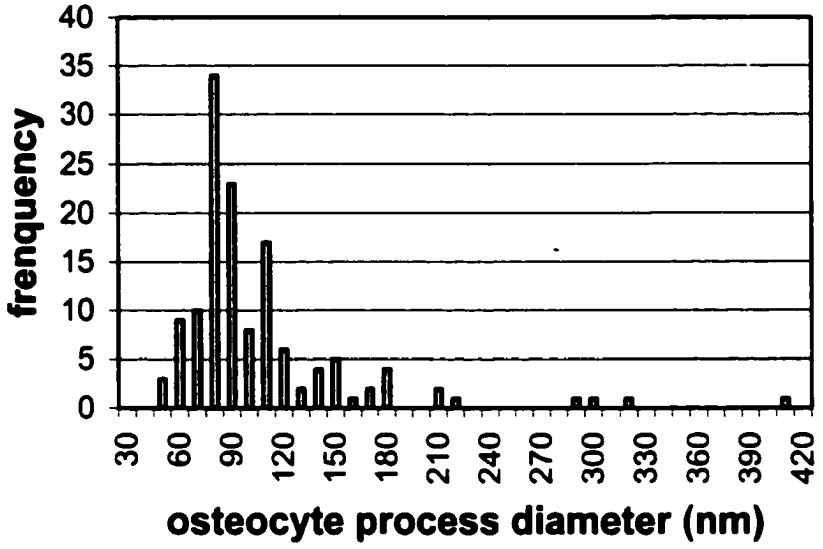

A

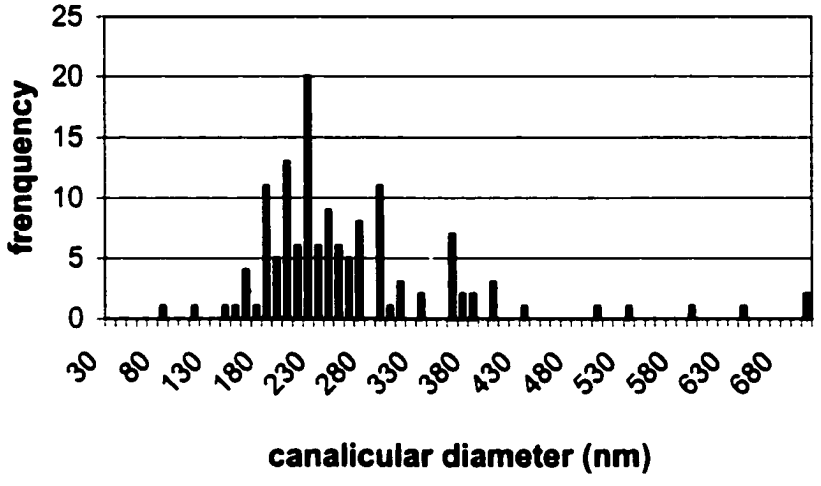

B

Figure 3.3 Measurements of osteocyte process and canalicular diameters. A. process diameter, n=137; B. canalicular diameter, n=137.

Figure 3.4 Electron photomicrograph of a longitudinal section through an osteocyte process. A: cell process; B: canalicular wall. C: transverse elements connecting process to canalicular wall; D: pericellular matrix filling the annular space. Paraformaldehyde-glutaraldehyde-RHT fixed. Bar = 200 nm

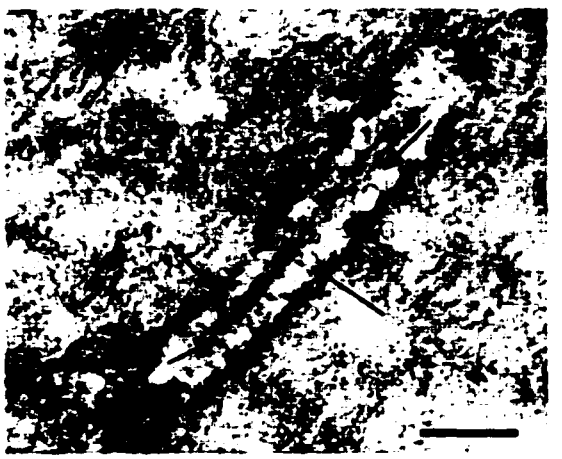

Figure 3.5 Electron photomicrograph showing the longitudinal section of an osteocyte process. Numerous transverse elements (arrows) can be seen extending from the cell process to the bony wall. Paraformaldehyde-glutaraldehyde-RHT fixed. Bar = 300 nm.

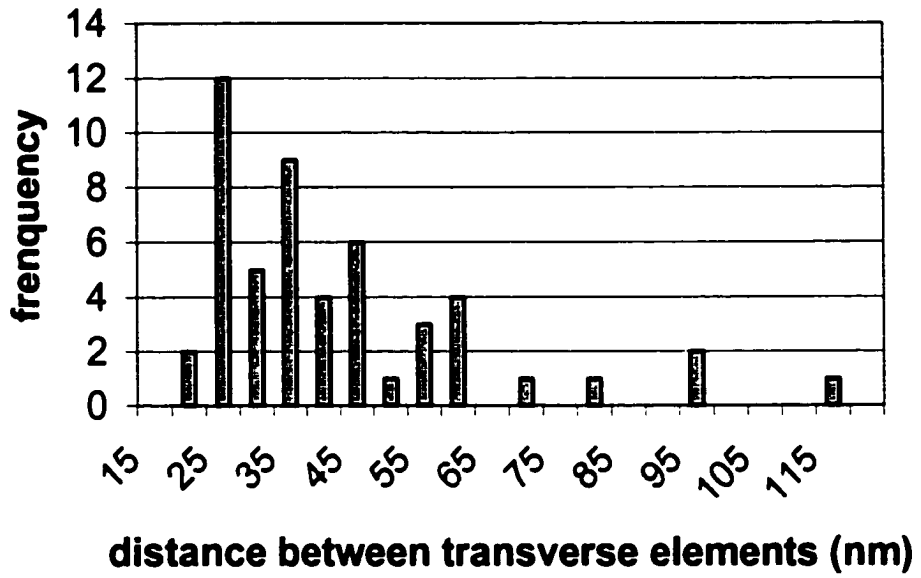

A

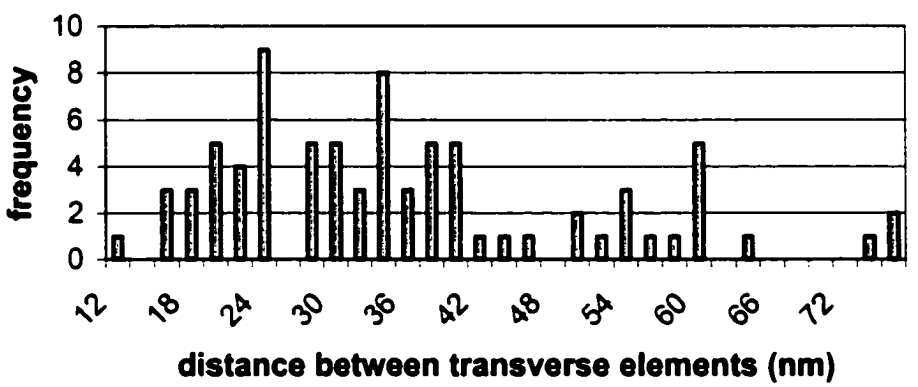

B

Figure 3.6 Measurements of spacing between transverse elements in the pericellular space surrounding the osteocytic process. A: cross section, n=53 ; B: longitudinal section, n=84.

Figure 3.7 Electron photomicrograph showing cross section of an osteocyte process. Darkened circular spots (see arrow) are cross-sections of cytoskeletal filaments ~6-8 nm in diameter, consistent with the size of actin filaments. Bar = 100 nm

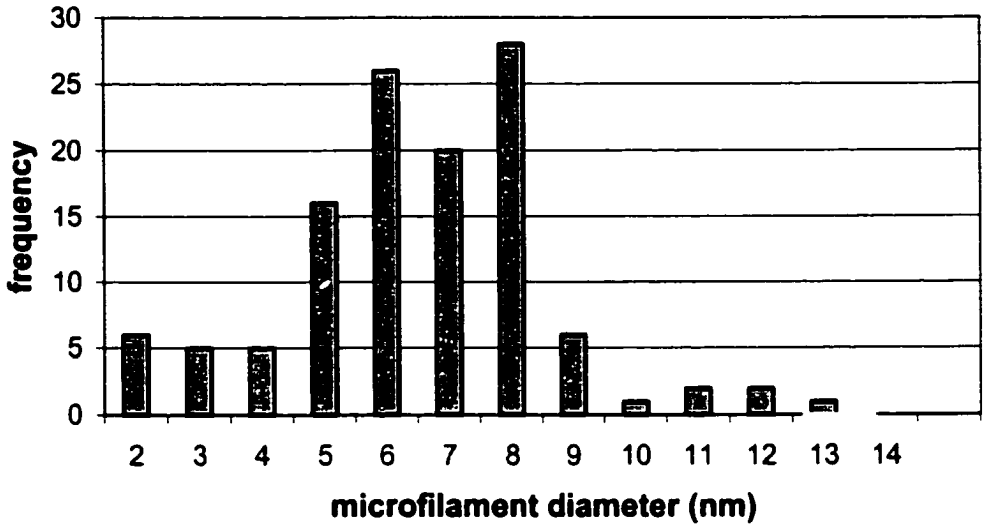

Figure 3.8 Measurements of the diameter of the microfilaments in the osteocyte processes. $n = 127$.

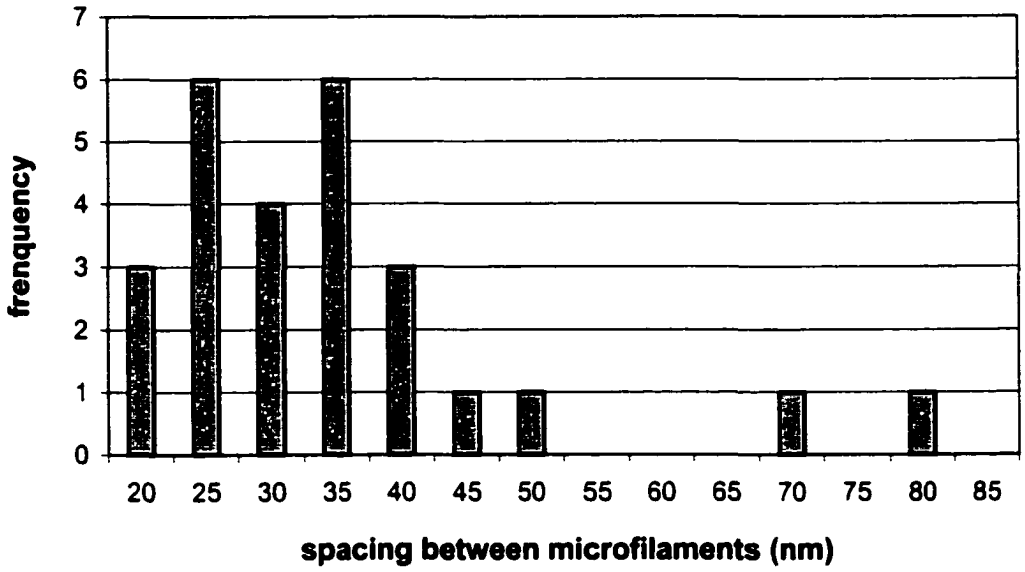

Figure 3.9 Measurements of spacing between the microfilaments in the osteocyte processes. $n = 27$.

Bone	b (nm)	a (nm)	$\frac{b-a}{2}$ (nm)	Sources
Human tibia, various ages	~ 700			Fig. 6, 7. (Marotti *et al.*, 1979)
15 day old chick	~ 400	~ 200	~ 100	Fig. 3.22. (Palumbo, 1986)
New born rabbit	~ 125			Fig. 1. (Palumbo *et al.*, 1990)
New born rabbit	~ 200			Fig. 10. (Palumbo *et al.*, 1990)
Human compact bone	~ 100			Fig. 19a. (Marotti, 1996)
Human compact bone	~ 200			Fig. 19b. (Marotti, 1996)
Human compact bone	~ 300			Fig. 20. (Marotti, 1996)

Table 3.1. Estimated values for the diameters of the canaliculi and the osteocyte processes taken from EM micrographs in the literature. b is the estimated value of the canalicular diameter, and a is the estimated value of osteocyte process diameter. $\frac{b-a}{2}$ is the width of the pericellular annulus.

Canalicular (dia.)	Process (dia.)	pericellular space (width)	Sources
85 – 100 nm		14 – 100 nm	Cooper *et al.*, 1966
150-550 nm			Marotti, 1990
150 – 550 nm	80 – 100 nm	25 – 235 nm	Marotti *et al.*, 1990
150 – 200 nm			Steflik *et al.*, 1994 (Fig. 11, 13)

Table 3.2. Summary of the values of the dimensions of the canaliculi, the osteocyte processes, and the pericellular space appearing in the literature.

Chapter 4. Concluding Remarks

4.1 Introduction

A new potential mechanism for mechanotransduction and strain amplification in bone was presented in this dissertation. The model for this mechanism provides an innovative conceptual view as to how bone fluid flow leads to the amplification at the cellular level of the mechanical strain experienced at the whole bone level. The background for this development was described in Chapter 1. The strain amplification model proposed was explained in Chapter 2. The experimental confirmation of the existence of several basic microanatomical features postulated in the strain amplification model was described in Chapter 3. The purpose of the present chapter is to summarize the accomplishments, describe the limitations of the accomplishments, and suggest future studies.

4.2 Summary of the Accomplishments

A possible model to explain how strain amplification occurs in bone was presented in Chapter 2. This strain amplification model predicted that the small deformation induced by mechanical loading exerted on the whole bone can be amplified by at least one order of magnitude at the cellular level of bone. This amplified level of strain is sensed by the osteocytes embedded in the bone tissue matrix. The key structural element in this strain amplification model is the tethering filaments between the osteocytic cell process and the

canalicular wall. Bone fluid flow through the pericellular space surrounding the osteocytic cell process, a space assumed to be filled with the tethering filaments, generates a drag force on the filaments. This drag force is transmitted to the actin cytoskeletal structure within the cell process via the transverse tethering filaments and transmembrane proteins. It was shown that a stimulus of relatively small deformation on the bone surface can be greatly amplified at the level of the cell process cytoskeleton by this mechanism. However, this behavior depends on several assumed microanatomical structures.

Specifically, the validity of this strain amplification model depends upon several assumptions concerning the microanatomy of bone and upon some assumed bone microanatomy parameter values. The model is based on the following assumptions: 1) there is a pericellular space surrounding the osteocyte process and a pericellular matrix fills this entire space; 2) the fiber spacing of the pericellular matrix is approximately 7 nm so that it can serve as a molecular sieve for albumin; 3) transverse elements exist in the pericellular space and these elements tether the osteocyte process to the canalicular wall; 4) there is a densely packed actin filament bundle that extends the entire length of the osteocyte cell process; 5) the intracellular actin bundle is connected to the pericellular matrix by transmembrane protein(s) and possibly other linker molecules. The parameter values required in the strain amplification model are: 1) the dimensions of the canaliculi, the osteocyte cell process and the pericellular space; 2) the spacing between the transverse tethering elements; 3) the spacing between the axial actin filaments; and 4) the spacing between the linker molecules that connect these axial microfilaments. The sensitivity analysis in Chapter 2 shows that the model predictions are not very sensitive to the fiber spacing of the pericellular matrix, the spacing between the transverse elements in the

pericellular matrix or to the axial actin filament spacing, but the model predictions are rather sensitive to the spacing between the cross-linker molecules in the actin filament bundle. The decrease of this latter spacing will decrease the strain amplification dramatically.

Several of the bone microanatomical structures assumed in the model have been observed previously in young animals. However, it is unclear whether these microanatomical structures also exist in mature animals. Furthermore, there are no quantitative studies in the literature for some of the parameter values assumed for the model. Therefore, we initiated experimental studies to examine these structural features in the mature bone of the mouse.

The key assumptions and the parameter values assumed in the strain amplification model were experimentally studied using ultrastructural techniques that were applied to bone for the first time. These studies were described in Chapter 3. Mature female mouse cortical bones were examined and the existence of the following structures were verified: 1) a pericellular space surrounding the osteocyte process with a pericellular matrix filling the entire space; 2) transverse elements tethering the osteocyte process and the canalicular wall; and 3) a densely packed microfilament bundle that extends the entire length of the osteocyte process. All of these microanatomical structures were observed for the first time in a mature animal. We also measured: 1) the dimensions of the canaliculi, the osteocytic cell process and the pericellular space; 2) the spacing between the transverse elements; and 3) the spacing between the axial microfilaments in the osteocyte process. All these measured values are in reasonable agreement with the parameter values applied in the strain amplification model. These measurements provide the critical input data for all

theoretical models involving fluid flow in a lacuno-canalicular system. The verification of these structural features provides strong support for the key assumptions used in the theoretical model in Chapter 2.

4.3 Limitations and Future Studies

There are several limitations in this study: 1) The possibility of a mechanotransduction mechanism in the osteocytic cell body was not considered; 2) A number of differences between *in vitro* and *in vivo* conditions (including cell growth in culture, nutrient transport, differing cellular matrix attachment in 2-D culture versus 3-D tissue) were not considered; 3) The calculation of shear stress and drag force was based on the existence of Haversian canals while the experimental study was conducted in mouse cortical bone that does not have a Haversian system; 4) The connections between the tethering filaments, the transmembrane proteins and the intracellular structure have not been confirmed; 5) The molecular identity of the tethering elements need to be determined; 6) The microfilaments observed in the process are believed to be actin filament but this needs to be confirmed; 7) The spacing of the fibers that form the molecular sieve in the pericellular matrix can only be roughly estimated by existing tracer studies; 8) The spacing between the linker molecules of the actin filament bundle has only been estimated for cells in culture; 9) Only one animal species, the mouse, has been studied. A discussion of these limitations and the possible future studies are given below.

The mechanosensation site in the strain amplification model (Chapter 2) was considered to be on the osteocytic cell process, and the possibility of mechanosensation site on the cell body was not considered in the present form of the model. Support for this

assumption comes from reports of the stretch activated channels occurring only the cell process and not in the cell body (Mikuni-Takagaki *et al.*, 1996; Mikuni-Takagaki, 1999). Mechanosensation sites on the cell body were not considered for this reason and because, it was thought, that the large space between the osteocytic cell membrane and the lacunar wall would lead to low shear stresses on the osteocytic cell membrane. However, if the osteocytic cell body was also connected to the lacunar wall by tethering elements, a similar mechanotransduction would occur in the cell body if its cytoskeleton were indeed soft. (Of course transverse fibers between the osteocytic cell body and the lacunar wall suggest a stiffer osteocytic cell body because they would provide a tension on the cytoskeleton within the osteocytic cell body. Furthermore, logical structural reasons would suggest that the cytoskeletons from the numerous osteocytic cell processes would connect to each other within the osteocytic cell body and make the body stiffer.) However, if the osteocytic cell body was indeed soft, it could be deformed greatly when subjected to a even low drag force resulting from the low speed fluid flow in lacunae. Further investigation is required to clarify whether there are connections between the osteocytic cell body and the lacunar wall so that the role that the osteocyte cell body plays in mechanotransduction in bone can be better understood.

The calculation of shear stress and drag force in this study is based on a model for osteonal bone. However, our experimental observations were conducted on the mouse, which does not have Haversian systems. It is unclear whether the basic structural features observed are the same in bone tissue with and without Haversian systems or whether the parameter values describing these ultrastructural features in the mouse are in the same range in other animals. Future experimental observations should be obtained for bone from

animals with Haversian systems. There is a wide variation in the measured parameter values in this study. Furthermore, the measured values from micrographs in the literature also vary greatly (Tables 3.1 and 3.2). Further investigation is necessary to clarify whether the variation is due to intrinsic bone properties or due to the sampling method. Bones from other species should be studied in the future to provide comparative data for the model.

This study was inspired by a paradox between in vitro observations that the large cellular deformations are required to induce intracellular biochemical response, and the *in vivo* observations that rather small whole tissue deformations lead to bone adaptation responses. However, other differences between *in vitro* and *in vivo* environments exist and they have not been accounted for. For example, the different mechanisms of nutrient transport in 2-D culture versus 3-D tissue, and the different cellular matrix attachment arrangements in 2-D culture and 3-D tissue were not considered. It is possible that these factors could contribute greatly to the different responses that bone cells exhibit at the same magnitude of deformation. However, one might note that other connective tissues cells, such as fibroblasts in fibrous tissue and chondrocytes in cartilage, respond to the same level of deformation (~15%) in 2-D culture and 3-D tissue (Almekinders *et al.*, 1993; Guilak *et al.*, 1995). Therefore, the large deformation required to activate osteocytes seems reasonable. However, in the future, these factors should be considered in the model. Efforts should be made towards constructing a more realistic environment for cell growth in culture (e.g., building a 3-D attachment environment).

It is hypothesized that a number of molecules, including CD44, various integrins, and HA, could serve as the tethering filaments between the osteocytic cell membrane and the canalicular wall. These different molecules have different mechanical properties and,

therefore, will influence the model predictions by introducing different bending moduli into the modeling of transverse element deformations. In the strain amplification model, it was assumed that these tethering filaments have no bending stiffness. It is thought that these macromolecules are much more flexible in bending than in axial stretching. Therefore, as a first approximation, the simplification employed in the strain amplification model to neglect the bending stiffness of the transverse elements may be reasonable. However, to further refine the strain amplification model, it is necessary to identify these molecules and introduce their mechanical properties into the calculation.

Although the electron micrograph shown in Fig. 3.1 strongly suggest the existence of the connections, their presence has not yet been confirmed. CD44 and various integrins have been located on the osteocyte membrane. CD44 is known to be the main receptor for hyaluronan (HA) and its cytoplasmic tail can combine with actin filaments. In future studies, immuno-histochemical techniques should be applied to co-localized the HA, CD44 and actin filament bundle within the cell process or the integrins and their corresponding ligands to confirm the presence of such a connection.

The spacing of the pericellular matrix is a key parameter in the strain amplification model. There is a body of indirect evidence from tracer studies (Knothe Tate *et al.*, 1998; Knothe Tate and Knothe, 2000; Knothe Tate *et al.*, 2001; Wang *et al.*, 2002) and the model analysis (Weinbaum *et al.*, 1994; Cowin *et al.*, 1995) suggesting that the fiber spacing of the pericellular matrix is approximately 7 nm. The usual spacing in biological matrices is typically about 5 to 25 nm; this range of values falls in the range of fiber spacing used here to induce large strain amplification in the sensitivity analysis. However, to fully support the strain amplification model, more direct evidence for this fiber spacing is required. Two

potential ways of studying this issue are: 1) Using immunofluorescent techniques, through which we can obtain the spacing of the matrix from the known molecular structure of the identified molecule; 2) Using new fixation techniques, through which detailed pericellular matrix structure may be preserved so that the spacing can be visualized and measured directly. Rostgaard *et al.* (1993) reported that, using an oxygen carrying fixative perfusion techniques, better preservation of ultrastructure could be obtained. Future studies could use these two techniques to better understand the spacing of the pericellular matrix.

Only densely packed microfilaments in the osteocytic process were observed in the experimental study on the actin filament bundle inside the osteocytic cell process reported in Chapter 3. The filaments' average diameter was measured to be ~ 6 nm, which is the typical value of the diameter of an actin filament. However, immunofluorescent techniques should be employed to confirm that these filaments in the osteocyte cell process are actin filaments.

The sensitivity analysis shows that the spacing between the linker molecules in the axial filament bundle is critical to the model prediction. In the future, immuno-electron microscopy techniques could be applied to stain the linker molecules and visualize the spacing between them. Sections might be cut thinner than 25 nm, the estimated spacing between the axial actin filaments, so that only one layer of linker molecules appears in each section.

In conclusion, the first quantitative model of mechanotransduction in bone has been presented. This model for the strain amplification system in bone tissue holds the potential to fundamentally impact the field of bone biology by illuminating the physiological mechanism of mechanosensation in bone. Although a few assumptions and parameter

values employed in the model have still not been confirmed or measured directly, the experimental observations have already verified the key structures and the key parameters that are employed in the strain amplification model. These new experiments support the proposed new strain amplification theory, but future experiments and a refined model are required to definitively confirm its validity.

Appendix

Appendix A: The calculation of the permeability k_p in the pericellular space

If the GAG side chains form a rectangular lattice that radiates fore and aft and laterally about the core protein (proteoglycan) at intervals Δ along its length (see Fig. 2.2a,b), the total length of GAG associated with each core protein is $\frac{s}{\Delta}(4l_{GAG})$, where s is the length of the core protein and l_{GAG} is the length of the GAG side chains. Since we have assumed $\Delta = 7nm$ and $l_{GAG} = 20nm$, the length ratio between the GAG side chains and the core proteins, $r_l = 4l_{GAG}/\Delta >> 1$, which suggests that the length of the GAG far exceeds that of the core protein. The drag on the core protein is thus largely due to its GAG side chains which, for simplicity, are arranged either transverse or parallel to the flow with equal length. The weighted hydraulic resistance due to the GAG plus the core protein is thus given by

$$\frac{1}{k_p} = \frac{r_l}{r_l+1}\left(\frac{1}{2k_{p1}} + \frac{1}{2k_{p2}}\right) + \frac{1}{r_l+1}\left(\frac{1}{k_{p1}}\right), \qquad \text{(A1)}$$

where k_{p1} is the Darcy permeability of the transverse fibers including the core proteins and k_{p2} the axial fibers. The expression for k_{p1} is given in Tsay and Weinbaum (*J. Fluid Mech.* 226, 125-148, 1991) as

$$k_{p1} = 0.0572 a_0^2 \left(\frac{\Delta}{a_0} \right)^{2.377}, \tag{A2}$$

The expression for k_{p2} is given in Cowin *et al.* (1995) as

$$k_{p2} = 0.147 a_0^2 \left(\frac{\Delta}{a_0} \right)^{2.285}. \tag{A3}$$

APPENDIX B. The method for estimating the Young's modulus of the cytoskeleton structure, E^*, in the radial direction

The purpose of this appendix is to describe the derivation associated with the estimate of 487.2 kPa for the Young's modulus of the cell process IAC. The derivation was illustrated in Figs. 2.2c in Chapter 2 and Figs. B1 and B2 in this appendix. The longitudinal actin filaments are modeled as infinitely long continuous beams. The outer filaments beneath process membrane (Fig. B1b) have a continuously distributed load representing the load transmitted by the transverse elements in the pericellular matrix, whereas the inner ones have point force loads, P, transmitted by the fimbrin cross-links (Fig. B1a). The (fimbrin) links between these infinitely long beams are considered to be rigid because the deflection of the actin filament, which is loaded transversely, will be much larger than the strain of the fimbrin linker molecules which are loaded axially. The radial deflection of the cell process cytoskeletal structure illustrated in Fig. 2.2c is $\bar{\delta} = \bar{\delta}_1 + 2\bar{\delta}_2 + \bar{\delta}_3$, where the $\bar{\delta}_i$, $i = 1,2,3$, are illustrated in Fig. B1. The bar is superimposed upon these deflections to indicate that they are average, or mean, deflections. The gage length over which the deflection occurs is $2l_1$, where l_1 is illustrated in Fig. B1, and the radial strain is given by $\varepsilon = \bar{\delta} / 2l_1$. It follows from Hooke's law that this strain is related to the stress σ by $E^* = \sigma / \varepsilon$, and it is the value of the Young's modulus E^* that we seek in this calculation.

The stress σ may also be expressed in terms of quantities illustrated in Fig. 2.2c, namely the length l_1, the length l_2 and the distributed load w per unit length: $\sigma = \frac{w \times l_2 \times 8}{l_2 \times 2\pi \times 2l_1}$.

Combining these results to obtain an expression for E^*, we find that E^* can expressed in terms of the three mean deflections and the known distributed loading w. Thus

$$E^* = \frac{4w/\pi}{\bar{\delta}_1 + 2\bar{\delta}_2 + \bar{\delta}_3}. \tag{B1}$$

This result reduces the determination of E^* to the determination of the three $\bar{\delta}_i$, $i = 1,2,3$. The determination of these quantities is described in the next paragraph.

The theory used for the determination of the three $\bar{\delta}_i$, $i = 1,2,3$, is classical beam theory. The fourth order differential equation governing the deflection y of the a beam is given by

$$EI\frac{d^4y}{dx^4} = w, \tag{B2}$$

where E is the Young's modulus of the beam material, I is the area moment of inertia of the cross-sectional area about a centroidal axis, $w(x)$ is the distributed load along the beam and x is the coordinate running along the longitudinal axis of the beam. The product EI is the flexural rigidity. We apply Eq.(B2) and the associated theory to the continuous infinite beam models of Fig. B1 to determine the three quantities, $\bar{\delta}_i$, $i = 1,2,3$. Consider first the continuous infinite beam model of Fig. B1a. For this beam $w(x) = 0$ (see Fig. B2a) and there are three geometric boundary conditions for this beam, namely that the slope at 0 and l, or at $n \times l$ (where n is any integer), is zero and the deflections at 0 and l are of opposite sign. Since Eq. (B2) is a fourth order ordinary differential equation, a fourth boundary condition is needed. This must be a force - or a moment - related condition because all the

symmetry in the situation has been exploited with the geometric boundary conditions. However, it is not obvious from elementary beam theory how one might obtain the fourth condition, the one related to a force or a moment, due to the fact that the beam is infinite in length. Actually the long length of the beam is the key to the solution because the equation of three moments (Timoshenko, and Young, 1945, *Theory of Structures*, McGraw Hill, New York, pp. 343.) may be used to find the moment at a point of application of the cross-link force. The moment is found to be the magnitude of $\frac{p \times l_2}{2}$, or $\frac{w}{2}$. Note from Fig. 2c that the force P must be equal to $w \times l_2$. The mean deflections, which are equal, are then given by

$$\bar{\delta}_1 = \bar{\delta}_2 = \frac{5pl_2^3}{3072EI}. \tag{B3}$$

This result gives the deflections $\bar{\delta}_i$, $i = 1,2$, in terms of the flexural rigidity EI of the longitudinal actin filament, the force $p = w \times l_2$ that the fimbrin cross-link exerts transversely on the infinite beam, and the length l_2.

We also need to determine a similar formula for $\bar{\delta}_3$. To that end we consider the continuous infinite beam model of Fig. B1b. For this beam $w(x) = w$ (a constant) (see Figure B2b) and the three geometric boundary conditions for this beam are the same as they were for the beam in Fig. B1a. The equation of three moments again supplies the missing condition, the moment at a point of application of the force P. The moment is found to be equal to $w \times l_2^2 / 12$. The mean deflection is then given by

$$\bar{\delta}_3 = \frac{Pl_2^3}{720EI}, \tag{B4}$$

This result gives the deflection $\overline{\delta}_3$, in terms of the flexural rigidity EI of the longitudinal actin filament, the force $P = w \times l_2$ that the fimbrin cross-link exerts transversely on the infinite beam, and the length l_2. Substituting the results (B3) and (B4) into (B5) a reduced expression for the desired E^* is obtained:

$$E^* = \frac{203EI}{l_2^4}. \qquad \text{(B5)}$$

(a)

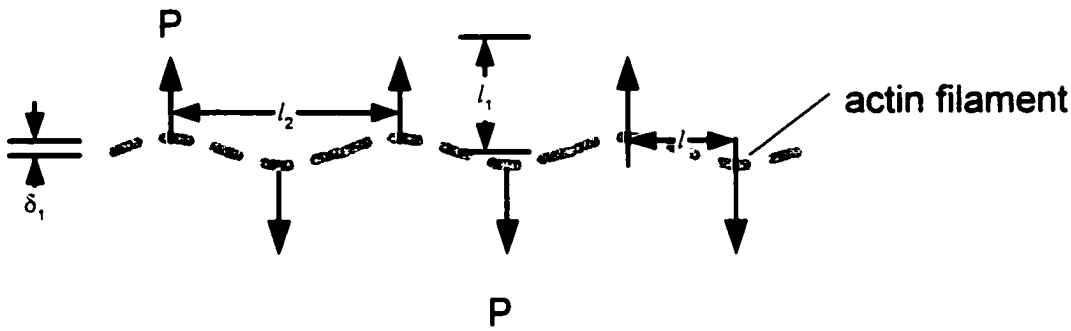

(b)

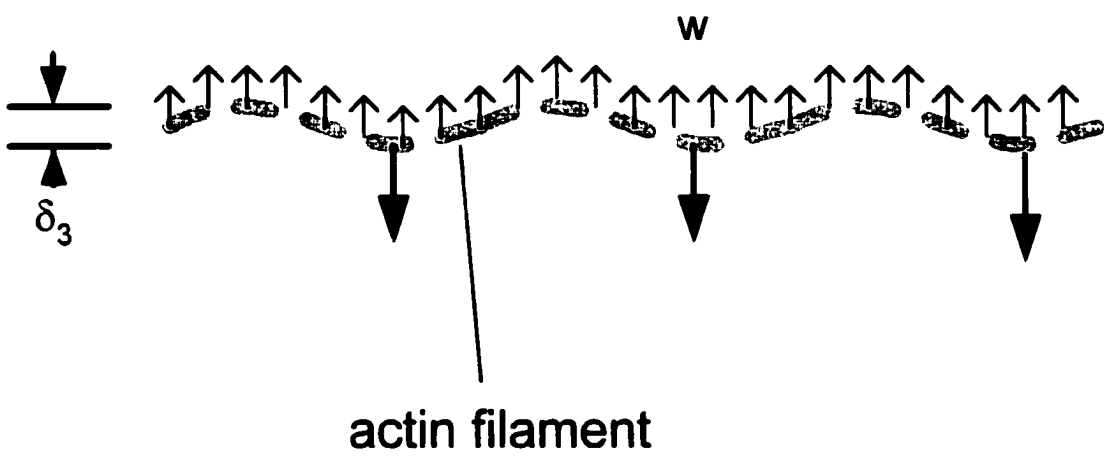

Figure B1: Illustration of the longitudinal actin filaments modeled as continuous infinite beams with two types of loadings; the two types of loadings are illustrated in (a) and (b). (a) A typical longitudinal actin filament in the interior portion of the cell process cytoskeletal structure where the load is applied by the fimbrin cross-links in alternate directions in a staggered fashion. (b) This continuous infinite beam models an exterior longitudinal actin filament. It is loaded in one direction by the fimbrin cross links and in the other direction by a continuously distributed load representing the applied external loading due to the extracellular matrix.

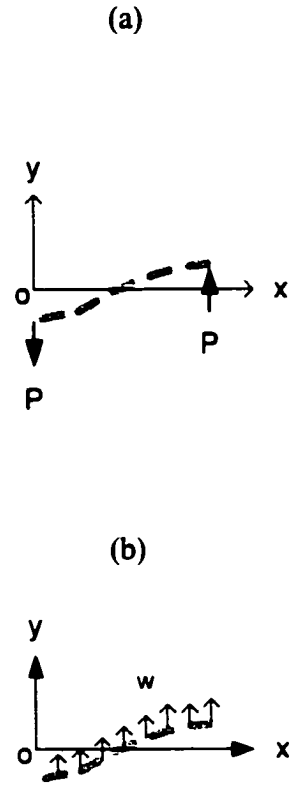

Figure B2: Illustration of the unit length of the longitudinal actin filaments modeled as continuous infinite beams with the two types of loading, the two types of loading described in Fig. B1. (a) A typical longitudinal actin filament in the interior portion of the cell process cytoskeletal structure loaded the fimbrin links in alternate directions in a staggered fashion. (b) This continuous infinite beam models a peripheral longitudinal actin filament beneath the process membrane. It is loaded in one direction by the fimbrin cross links and in the other direction by a continuously distributed load representing the applied external loading.

Bibliography

Aarden, E. M., A. M. Wassenaar, M. J. Alblas and P. J. Nijweide (1996). "Immunocytochemical demonstration of extracellular matrix proteins in isolated osteocytes." Histochem Cell Biol **106**(5): 495-501.

Almekinders, L. C., A. J. Banes and C. A. Ballenger (1993). "Effects of repetitive motion on human fibroblasts." Med Sci Sports Exerc **25**(5): 603-7.

Bretscher, A. and K. Weber (1980). "Fimbrin, a new microfilament-associated protein present in microvilli and other cell surface structures." J Cell Biol **86**(1): 335-40.

Buckley, M. J., A. J. Banes, L. G. Levin, B. E. Sumpio, M. Sato, R. Jordan, J. Gilbert, G. W. Link and R. Tran Son Tay (1988). "Osteoblasts increase their rate of division and align in response to cyclic, mechanical tension in vitro." Bone Miner **4**(3): 225-36.

Buckwalter, J. A. and L. C. Rosenberg (1982). "Electron microscopic studies of cartilage proteoglycans. Direct evidence for the variable length of the chondroitin sulfate-rich region of proteoglycan subunit core protein." J Biol Chem **257**(16): 9830-9.

Burger, E. H. and J. Klein-Nulend (1999). "Mechanotransduction in bone--role of the lacuno-canalicular network." Faseb J **13**(Suppl): S101-12.

Chailley, B., G. Nicolas and M. C. Laine (1989). "Organization of actin microfilaments in the apical border of oviduct ciliated cells." Biol Cell **67**(1): 81-90.

Cooper, R. R., J. W. Milgram and R. A. Robinson (1966). "Morphology of the osteon. An electron microscopic study." J Bone Joint Surg Am **48**(7): 1239-71.

Cowin, S. C., L. Moss-Salentijn and M. L. Moss (1991). "Candidates for the mechanosensory system in bone." J Biomech Eng **113**(2): 191-7.

Cowin, S. C. and S. Weinbaum (1998). "Strain amplification in the bone mechanosensory system." Am J Med Sci **316**(3): 184-8.

Cowin, S. C., S. Weinbaum and Y. Zeng (1995). "A case for bone canaliculi as the anatomical site of strain generated potentials." J Biomech **28**(11): 1281-97.

Curry, F. E. (1986). "Determinants of capillary permeability: a review of mechanisms based on single capillary studies in the frog." Circ Res **59**(4): 367-80.

Dupuis, D. E., W. H. Guilford, J. Wu and D. M. Warshaw (1997). "Actin filament mechanics in the laser trap." J Muscle Res Cell Motil **18**(1): 17-30.

Fritton, S. P., K. J. McLeod and C. T. Rubin (2000). "Quantifying the strain history of bone: spatial uniformity and self- similarity of low-magnitude strains." J Biomech **33**(3): 317-25.

Fritton, S. P. and C. Rubin (2001). Chapter 8. In Vivo Measurement of bone deformations using strains gauges. Bone Mechanics Handbook. S. C. Cowin, CRC Press.

Glenney, J. R., Jr., P. Kaulfus, P. Matsudaira and K. Weber (1981). "F-actin binding and bundling properties of fimbrin, a major cytoskeletal protein of microvillus core filaments." J Biol Chem **256**(17): 9283-8.

Gohel, A. R., A. R. Hand and G. A. Gronowicz (1995). "Immunogold localization of beta 1-integrin in bone: effect of glucocorticoids and insulin-like growth factor I on integrins and osteocyte formation." J Histochem Cytochem **43**(11): 1085-96.

Guilak, F., A. Ratcliffe and V. C. Mow (1995). "Chondrocyte deformation and local tissue strain in articular cartilage: a confocal microscopy study." J Orthop Res **13**(3): 410-21.

Guo, P., A. M. Weinstein and S. Weinbaum (2000). "A hydrodynamic mechanosensory hypothesis for brush border microvilli." Am J Physiol Renal Physiol **279**(4): F698-712.

Harrigan, T. P. and J. J. Hamilton (1993). "Bone strain sensation via transmembrane potential changes in surface osteoblasts: loading rate and microstructural implications." J Biomech **26**(2): 183-200.

Holtrop, M. E. (1975). "The ultrastructure of bone." Ann Clin Lab Sci **5**(4): 264-71.

Horwitz, A. F. (1997). "Integrins and health." Sci Am **276**(5): 68-75.

Hudspeth, A. J. (1992). "Hair-bundle mechanics and a model for mechanoelectrical transduction by hair cells." Soc Gen Physiol Ser **47**: 357-70.

Hughes, D. E., D. M. Salter and R. Simpson (1994). "CD44 expression in human bone: a novel marker of osteocytic differentiation." J Bone Miner Res **9**(1): 39-44.

Hung, C. T., S. R. Pollack, T. M. Reilly and C. T. Brighton (1995). "Real-time calcium response of cultured bone cells to fluid flow." Clin Orthop(313): 256-69.

Hunziker, E. B., W. Herrmann and R. K. Schenk (1982). "Improved cartilage fixation by ruthenium hexammine trichloride (RHT). A prerequisite for morphometry in growth cartilage." J Ultrastruct Res **81**(1): 1-12.

Jacobs, C. R., C. E. Yellowley, B. R. Davis, Z. Zhou, J. M. Cimbala and H. J. Donahue (1998). "Differential effect of steady versus oscillating flow on bone cells." J Biomech **31**(11): 969-76.

Jamal, H. H. and J. E. Aubin (1996). "CD44 expression in fetal rat bone: in vivo and in vitro analysis." Exp Cell Res **223**(2): 467-77.

Jande, S. S. and L. F. Belanger (1971). "Electron microscopy of osteocytes and the pericellular matrix in rat trabecular bone." Calcif Tissue Res **6**(4): 280-9.

King, G. J. and M. E. Holtrop (1975). "Actin-like filaments in bone cells of cultured mouse calvaria as demonstrated by binding to heavy meromyosin." J Cell Biol **66**(2): 445-51.

Kishino, A. and T. Yanagida (1988). "Force measurements by micromanipulation of a single actin filament by glass needles." Nature **334**(6177): 74-6.

Klein-Nulend, J., A. van der Plas, C. M. Semeins, N. E. Ajubi, J. A. Frangos, P. J. Nijweide and E. H. Burger (1995). "Sensitivity of osteocytes to biomechanical stress in vitro." Faseb J **9**(5): 441-5.

Knothe Tate, M., A. Tami, P. Nasser, R. Steck and M. Schaffler (2001). Permeability characteristics of different molecular tracers in loaded and unloaded bone. 47th Annual Meeting of Orthopaedic Research Society, San Francisco, California.

Knothe Tate, M. L. and U. Knothe (2000). "An ex vivo model to study transport processes and fluid flow in loaded bone." J Biomech **33**(2): 247-54.

Knothe Tate, M. L., U. Knothe and P. Niederer (1998). "Experimental elucidation of mechanical load-induced fluid flow and its potential role in bone metabolism and functional adaptation." Am J Med Sci **316**(3): 189-95.

Kufahl, R. H. and S. Saha (1990). "A theoretical model for stress-generated fluid flow in the canaliculi- lacunae network in bone tissue." J Biomech **23**(2): 171-80.

Lanyon, L. E., W. G. Hampson, A. E. Goodship and J. S. Shah (1975). "Bone deformation recorded in vivo from strain gauges attached to the human tibial shaft." Acta Orthop Scand **46**(2): 256-68.

Lodish, H. (1999). Molecular Cell Biology, W.H. Freeman and Company: 969-1003.

Marotti, G. (1990). Ultrastructure of skeletal tissue, Kluve Academic Publishers.

Marotti, G. (1996). "The structure of bone tissues and the cellular control of their deposition." Ital J Anat Embryol **101**(4): 25-79.

Marotti, G., V. Cane, S. Palazzini and C. Palumbo (1990). "Structure-function relationships in the osteocyte." Italian Journal of Mineral & Electrolyte Metabolism **4**(2): 93-106.

Marotti, G., N. Delrio, F. Marotti and M. Fadda (1979). "Quantitative analysis of the bone destroying activity of osteocytes and osteoclasts in experimental disuse osteoporosis." Ital J Orthop Traumatol **5**(2): 225-40.

McLeod, K. J., H. J. Donahue, P. E. Levin and C. T. Rubin (1991). Low frequency sinusoidal electric fields alter calcium fluctuations in osteoblast-like cells. Electromagnetics in biology and medicine. C. T. Brighton and S. R. Pollack. San Francisco, San Francisco: 111-115.

Mikuni-Takagaki, Y. (1999). "Mechanical responses and signal transduction pathways in stretched osteocytes." J Bone Miner Metab **17**(1): 57-60.

Mikuni-Takagaki, Y., Y. Suzuki, T. Kawase and S. Saito (1996). "Distinct responses of different populations of bone cells to mechanical stress." Endocrinology **137**(5): 2028-35.

Mooseker, M. S. and L. G. Tilney (1975). "Organization of an actin filament-membrane complex. Filament polarity and membrane attachment in the microvilli of intestinal epithelial cells." J Cell Biol **67**(3): 725-43.

Morey, E. R. and D. J. Baylink (1978). "Inhibition of bone formation during space flight." Science **201**(4361): 1138-41.

Murray, D. W. and N. Rushton (1990). "The effect of strain on bone cell prostaglandin E2 release: a new experimental method." Calcif Tissue Int **47**(1): 35-9.

Nakamura, H., S. Kenmotsu, H. Sakai and H. Ozawa (1995). "Localization of CD44, the hyaluronate receptor, on the plasma membrane of osteocytes and osteoclasts in rat tibiae." Cell Tissue Res **280**(2): 225-33.

Nakamura, H. and H. Ozawa (1996). "Immunolocalization of CD44 and the ERM family in bone cells of mouse tibiae." J Bone Miner Res **11**(11): 1715-22.

Noonan, K. J., J. W. Stevens, R. Tammi, M. Tammi, J. A. Hernandez and R. J. Midura (1996). "Spatial distribution of CD44 and hyaluronan in the proximal tibia of the growing rat." J Orthop Res **14**(4): 573-81.

Oosawa, F. (1977). "Actin-actin bond strength and the conformational change of F-actin." Biorheology **14**(1): 11-19.

Otter, M. W., V. R. Palmieri, D. D. Wu, K. G. Seiz, L. A. MacGinitie and G. V. Cochran (1992). "A comparative analysis of streaming potentials in vivo and in vitro." J Orthop Res **10**(5): 710-9.

Owan, I., D. B. Burr, C. H. Turner, J. Qiu, Y. Tu, J. E. Onyia and R. L. Duncan (1997). "Mechanotransduction in bone: osteoblasts are more responsive to fluid forces than mechanical strain." Am J Physiol **273**(3 Pt 1): C810-5.

Owen, M. and J. T. Triffitt (1976). "Extravascular albumin in bone tissue." J Physiol **257**(2): 293-307.

Palumbo, C. (1986). "A three-dimensional ultrastructural study of osteoid-osteocytes in the tibia of chick embryos." Cell Tissue Res **246**(1): 125-31.

Palumbo, C., S. Palazzini and G. Marotti (1990). "Morphological study of intercellular junctions during osteocyte differentiation." Bone **11**(6): 401-6.

Palumbo, C., S. Palazzini, D. Zaffe and G. Marotti (1990). "Osteocyte differentiation in the tibia of newborn rabbit: an ultrastructural study of the formation of cytoplasmic processes." Acta Anat **137**(4): 350-8.

Piekarski, K. and M. Munro (1977). "Transport mechanism operating between blood supply and osteocytes in long bones." Nature **269**(5623): 80-2.

Pitsillides, A. A., S. C. Rawlinson, R. F. Suswillo, S. Bourrin, G. Zaman and L. E. Lanyon (1995). "Mechanical strain-induced NO production by bone cells: a possible role in adaptive bone (re)modeling?" Faseb J **9**(15): 1614-22.

Reich, K. M. and J. A. Frangos (1991). "Effect of flow on prostaglandin E2 and inositol trisphosphate levels in osteoblasts." Am J Physiol **261**(3 Pt 1): C428-32.

Rostgaard, J., K. Qvortrup and S. S. Poulsen (1993). "Improvements in the technique of vascular perfusion-fixation employing a fluorocarbon-containing perfusate and a peristaltic pump controlled by pressure feedback." J Microsc **172**(Pt 2): 137-51.

Rubin, C. and K. J. McLeod (1996). Inhibition of osteopenia by biophysical intervention. Osteoporosis. R. Marcus, D. Eklman and J. Kelsey. New York, Academic Press: pp. 351-371.

Rubin, C. T. and L. E. Lanyon (1984). "Regulation of bone formation by applied dynamic loads." J Bone Joint Surg Am **66**(3): 397-402.

Salzstein, R. A. and S. R. Pollack (1987). "Electromechanical potentials in cortical bone--II. Experimental analysis." J Biomech **20**(3): 271-80.

Salzstein, R. A., S. R. Pollack, A. F. Mak and N. Petrov (1987). "Electromechanical potentials in cortical bone--I. A continuum approach." J Biomech **20**(3): 261-70.

Satcher, R. L., Jr. and C. F. Dewey, Jr. (1996). "Theoretical estimates of mechanical properties of the endothelial cell cytoskeleton." Biophys J **71**(1): 109-18.

Sauren, Y. M., R. H. Mieremet, C. G. Groot and J. P. Scherft (1992). "An electron microscopic study on the presence of proteoglycans in the mineralized matrix of rat and human compact lamellar bone." Anat Rec **232**(1): 36-44.

Scott, G. C. and E. Korostoff (1990). "Oscillatory and step response electromechanical phenomena in human and bovine bone." J Biomech **23**(2): 127-43.

Sessions, N. D., B. P. Halloran, D. D. Bikle, T. J. Wronski, C. M. Cone and E. Morey-Holton (1989). "Bone response to normal weight bearing after a period of skeletal unloading." Am J Physiol **257**(4 Pt 1): E606-10.

Shapiro, F., C. Cahill, G. Malatantis and R. C. Nayak (1995). "Transmission electron microscopic demonstration of vimentin in rat osteoblast and osteocyte cell bodies and processes using the immunogold technique." Anat Rec **241**(1): 39-48.

Shin, D. and K. Athanasiou (1999). "Cytoindentation for obtaining cell biomechanical properties." J Orthop Res **17**(6): 880-90.

Stanford, C. M., J. W. Stevens and R. A. Brand (1995). "Cellular deformation reversibly depresses RT-PCR detectable levels of bone-related mRNA." J Biomech **28**(12): 1419-27.

Starkebaum, W., S. R. Pollack and E. Korostoff (1979). "Microelectrode studies of stress-generated potentials in four-point bending of bone." J Biomed Mater Res **13**(5): 729-51.

Steflik, D. E., A. L. Sisk, G. R. Parr, F. T. Lake, P. J. Hanes, D. J. Berkery and P. Brewer (1994). "Transmission electron and high-voltage electron microscopy of osteocyte cellular processes extending to the dental implant surface." J Biomed Mater Res **28**(9): 1095-107.

Tanaka-Kamioka, K., H. Kamioka, H. Ris and S. S. Lim (1998). "Osteocyte shape is dependent on actin filaments and osteocyte processes are unique actin-rich projections." J Bone Miner Res **13**(10): 1555-68.

Toma, C. D., S. Ashkar, M. L. Gray, J. L. Schaffer and L. C. Gerstenfeld (1997). "Signal transduction of mechanical stimuli is dependent on microfilament integrity: identification of osteopontin as a mechanically induced gene in osteoblasts." J Bone Miner Res **12**(10): 1626-36.

Wang, L., S. C. Cowin, S. Weinbaum and S. P. Fritton (2000). "Modeling tracer transport in an osteon under cyclic loading." Ann Biomed Eng **28**(10): 1200-9.

Wang, L., S. C. Cowin, S. Weinbaum and S. P. Fritton (2001). "In response to "Mixing mechanisms and net solute transport in bone" by M.L. Knothe Tate." Annals of Biomedical Engineering **29**: pp. 812-816.

Wang, L., S. B. Doty and S. P. Fritton (2002). "Perfusing porous bone matrix using varied sized molecular tracers." Bone **submitted**.

Wang, L., S. P. Fritton, S. C. Cowin and S. Weinbaum (1999). "Fluid pressure relaxation depends upon osteonal microstructure: modeling an oscillatory bending experiment." J Biomech **32**(7): 663-72.

Wassermann, F. and J. Yaeger (1965). "Fine structure of osteocyte capsule and of wall of lacunae in bone." Zeitschrift fur Zellforschung **67**(5): 636-652.

Weinbaum, S. (1998). "1997 Whitaker Distinguished Lecture: Models to solve mysteries in biomechanics at the cellular level; a new view of fiber matrix layers." Ann Biomed Eng **26**(4): 627-43.

Weinbaum, S., S. C. Cowin and Y. Zeng (1994). "A model for the excitation of osteocytes by mechanical loading-induced bone fluid shear stresses." J Biomech **27**(3): 339-60.

Weinbaum, S., P. Guo and L. You (2001). "A new view of mechanotransduction and strain amplification in cells with microvilli and cell processes." Biorheology **38**(2-3): 119-42.

Weinger, J. M. and M. E. Holtrop (1974). "An ultrastructural study of bone cells: the occurrence of microtubules, microfilaments and tight junctions." Calcif Tissue Res **14**(1): 15-29.

Williams, J. L., J. P. Iannotti, A. Ham, J. Bleuit and J. H. Chen (1994). "Effects of fluid shear stress on bone cells." Biorheology **31**(2): 163-70.

You, J., G. C. Reilly, X. Zhen, C. E. Yellowley, Q. Chen, H. J. Donahue and C. R. Jacobs (2001). "Osteopontin gene regulation by oscillatory fluid flow via intracellular calcium mobilization and activation of mitogen-activated protein kinase in MC3T3-E1 osteoblasts." J Biol Chem **276**(16): 13365-71.

You, J., C. E. Yellowley, H. J. Donahue, Y. Zhang, Q. Chen and C. R. Jacobs (2000). "Substrate deformation levels associated with routine physical activity are less stimulatory to bone cells relative to loading-induced oscillatory fluid flow." J Biomech Eng **122**(4): 387-93.

You, L., S. C. Cowin, M. B. Schaffler and S. Weinbaum (2001). "A model for strain amplification in the actin cytoskeleton of osteocytes due to fluid drag on pericellular matrix." J Biomech **34**(11): 1375-86.

Zaman, G., R. F. Suswillo, M. Z. Cheng, I. A. Tavares and L. E. Lanyon (1997). "Early responses to dynamic strain change and prostaglandins in bone- derived cells in culture." J Bone Miner Res **12**(5): 769-77.

Zeng, Y., S. C. Cowin and S. Weinbaum (1994). "A fiber matrix model for fluid flow and streaming potentials in the canaliculi of an osteon." Ann Biomed Eng **22**(3): 280-92.

Zhang, D., S. C. Cowin and S. Weinbaum (1997). "Electrical signal transmission and gap junction regulation in a bone cell network: a cable model for an osteon." Ann Biomed Eng **25**(2): 357-74.

Zhang, D., S. Weinbaum and S. C. Cowin (1998). "Electrical signal transmission in a bone cell network: the influence of a discrete gap junction." Ann Biomed Eng **26**(4): 644-59.